Universidade Federal de Minas Gerais (UFMG)
Av. Antônio Carlos 6627, CEP 31270-901,
Belo Horizonte, MG Brasil

DISSERTAÇÃO DE MESTRADO Nº 1128

Longitudinal Control Strategies for Unmanned Ground Vehicles in Uneven Terrains

Victor Ricardo Fernandes Miranda

Belo Horizonte
July 26, 2019

UNIVERSIDADE FEDERAL DE MINAS GERAIS
GRADUATE PROGRAM IN ELECTRICAL ENGINEERING

Longitudinal Control Strategies for Unmanned Ground Vehicles in Uneven Terrains

Thesis presented to the Graduate Program in Electrical Engineering of the Federal University of Minas Gerais as a partial requirement to obtain a Master's degree in Electrical Engineering.

Victor Ricardo Fernandes Miranda
Advisor: Leonardo Amaral Mozelli
Co-Advisor: Armando Alves Neto

Belo Horizonte
July 26, 2019

UNIVERSIDADE FEDERAL DE MINAS GERAIS
ESCOLA DE ENGENHARIA
PROGRAMA DE PÓS-GRADUAÇÃO EM ENGENHARIA ELÉTRICA

Estratégias de Controle Longitudinal para Veículos Terrestres Não Tripulados em Terrenos Irregulares

Dissertação de Mestrado submetida à Banca Examinadora designada pelo Colegiado do Programa de Pós-Graduação em Engenharia Elétrica da Universidade Gederal de Minas Gerais, como requisito para obtenção do Título de Mestre em Engenharia Elétrica.

Victor Ricardo Fernandes Miranda
Orientador: Leonardo Amaral Mozelli
Co-Orientador: Armando Alves Neto

Belo Horizonte
26 de Julho de 2019

Miranda, Victor Ricardo Fernandes.
M672e Estratégias de controle longitudinal para veículos terrestres não tripulados em terrenos irregulares [recurso eletrônico] / Victor Ricardo Fernandes Miranda. – 2019.
1 recurso online (70 f. : il., color.) : pdf.

Orientador: Leonardo Amaral Mozelli.
Coorientador: Armando Alves Neto.

Dissertação (mestrado) Universidade Federal de Minas Gerais, Escola de Engenharia.

Bibliografia: f. 65-70.
Exigências do sistema: Adobe Acrobat Reader.

1. Engenharia elétrica - Teses. 2. Veículos autônomos - Teses. 3. Controle robusto - Teses. 4. Teoria do controle não-linear -Teses. I. Mozelli, Leonardo Amaral. II. Alves Neto, Armando. III. Universidade Federal de Minas Gerais. Escola de Engenharia. IV. Título.

CDU: 621.3(043)

Ficha catalográfica: Biblioteca Profº Mário Werneck, Escola de Engenharia da UFMG

"Longitudinal Control Strategies For Unmanned Ground Vehicles In Uneven Terrains"

Victor Ricardo Fernandes Miranda

Dissertação de Mestrado submetida à Banca Examinadora designada pelo Colegiado do Programa de Pós-Graduação em Engenharia Elétrica da Escola de Engenharia da Universidade Federal de Minas Gerais, como requisito para obtenção do grau de Mestre em Engenharia Elétrica.

Aprovada em 26 de julho de 2019.

Por:

Prof. Dr. Leonardo Amaral Mozelli
DELT (UFMG) - Orientador

Prof. Dr. Armando Alves Neto
DELT (UFMG) - Coorientador

Prof. Dr. Gustavo Medeiros Freitas
DEE (UFMG)

Prof. Dr. João Pedro Hallack Sansão
DTECH (UFSJ - Campus Alto Paraopeba)

Prof. Dr. Víctor Costa da Silva Campos
DELT (UFMG)

ACKNOWLEDGEMENTS

First, I thank to my family. In special to my parents Geraldo Ricardo and Mariza, who always encouraged me and supported my choices, guiding me and transmitting all their experience. Thanks to you, all this was possible.

I am very grateful to my mentors Leonardo Mozelli and Armando Neto for their guidance in the last two years and for sharing their knowledge with me since college. Besides, I must thank the members of the examination committee, the professors Gustavo Freitas, João Pedro Sansão and Victor Costa, for sharing their valuable opinions and insightful comments, contributing to improve this work.

I thank the colleagues and employees of UFMG and of the School of Engineering. Thank to the members of the research groups D!FCON and MACRO. Specially the students from the CORO laboratory, for the friendship built.

Thanks to all the professors of the Graduate Program in Electrical Engineering (PPGEE), their teachings contributed to the conclusion of this work.

Finally, I acknowledge the financial support provided by CAPES and PPGEE.

RESUMO

VICTOR R. F. MIRANDA. **Longitudinal Control Strategies for Unmanned Ground Vehicles in Uneven Terrains**. 2019. 70 f. Master dissertation (Master student Engenharia Elétrica) – Escola de Engenharia (UFMG), Belo Horizonte – MG.

Este trabalho aborda estratégias de controle longitudinal para rastreamento de trajetórias de referência por um veículo terrestre não tripulado, considerando alterações no tipo e nas condições do terreno. Também apresenta a construção de uma plataforma móvel *off-road* de quatro rodas, com arquitetura *Ackermann*, em escala reduzida, para realização de tarefas em um ambiente de terreno irregular.

Em vários cenários de aplicação de um robô móvel terrestre, como nas tarefas de mineração e agricultura, deve-se trafegar por terrenos irregulares e não-estruturados. Isso pode afetar o desempenho do veículo durante a execução dessas tarefas em velocidades mais altas. Essas irregularidades no terreno, bem como mudanças no tipo do solo e alterações na carga transportada pelo robô, são distúrbios que afetam a dinâmica do robô, acarretando dificuldades no ponto de vista do controle de velocidade e navegação.

Tendo em vista esses problemas, propõe-se a construção de uma plataforma, que possibilite a sua utilização em terrenos irregulares, para realização de tarefas de forma semi-autônoma. Dessa forma, duas técnicas de controle em espaço de estados são abordadas visando reduzir o efeito dos distúrbios causados pelo terreno e por eventuais mudanças no robô durante a execução de uma tarefa: um controlador Robusto PID, sintonizado por meio de LMIs, e um controlador não linear, sintonizado por técnica *Backstepping* com ação integral no erro.

A plataforma construída foi equipada com sensores de baixo custo e um computador embarcado, possibilitando testes reais para avaliação do desempenho de cada controlador projetado.

Palavras-chave: Veículos Autônomos; Rastreamento de trajetória; Controle Robusto; Controle Não Linear; Robótica Móvel. .

ABSTRACT

VICTOR R. F. MIRANDA. **Longitudinal Control Strategies for Unmanned Ground Vehicles in Uneven Terrains**. 2019. 70 f. Master dissertation (Master student Engenharia Elétrica) – Escola de Engenharia (UFMG), Belo Horizonte – MG.

This work presents control strategies to track longitudinal trajectories by an unmanned ground vehicle, considering changes in terrain type and conditions. It also features the design and construction of a small, off-road, four-wheeled, Ackermann platform, able to travel in uneven terrains.

In several scenarios of mobile robot's application, as in mining and agriculture tasks, it is necessary to drive on irregular and unstructured terrains. This may directly affect the vehicle performance while executing these tasks at higher speeds. These terrain irregularities, as well as changes in the soil type and changes in the load carried by the robot, are disturbances that affect the robot dynamics, causing difficulties in the point of view of navigation and speed control.

In view of these problems, a simple platform was built, which can be used in irregular terrains, to perform semi-autonomous tasks. Thus, to achieve this autonomous tracking, this thesis proposes two control techniques to reduce the effect of ground disturbances and changes in the robot mass during the execution of a task: Robust PID controller, tuned by an LMI approach, and a nonlinear controller, tuned by a Backstepping technique, with integral action.

This platform is equipped with low-cost sensors and embedded computers. Simulation and real-life experiments are presented to illustrate the performance of each designed controller.

Keywords: Autonomous ground vehicle; Trajectory tracking; Robust control; Nonlinear control; Mobile Robots.

LIST OF FIGURES

LIST OF TABLES

LIST OF ABBREVIATIONS AND ACRONYMS

BMI	Bilinear Matrix Inequality
CLF	Control Lyapunov Function
ESC	Electronic Speed Controller
GPS	Global Positioning System
IAE	Integral Absolute Error
IMU	Inertial Measurement Unit
ISE	Integral Square Error
ITAE	Integral Time Absolute Error
ITSE	Integral Time Square Error
LMI	Linear Matrix Inequality
LQR	Linear Quadratic Regulator
MPC	Model Predictive Control
PID	Proportional-Integral-Derivative
PWM	Pulse Width Modulation
ROS	Robot Operating System
SMC	Sliding Mode Control
SOF	Static Output Feedback
SOF-PID	Proportional-Integral-Derivative Static Output Feedback
UAV	Unmanned Aerial Vehicle
UGV	Unmanned Ground Vehicle

CONTENTS

CHAPTER

1

INTRODUCTION

1.1 Motivation

Mobile Robotics has experienced substantial growth in the last decades, thanks to the wide applicability in civilian, industrial and military sectors. It is commonly associated with improvements in security, accuracy, agility and cost reduction in the execution of tasks.

The Unmanned Aerial Vehicles (UAVs) are commonly used in military and civil sectors for tasks such as reconnaissance, search and rescue, military defense, delivering medical supplies, patrol missions, journalism, among others, attracting researches as in Rudol and Doherty [2008] and Tomic et al. [2012]. Another possibility is to help in agricultural production, a strong industry in the primary sector, where autonomous UAVs are currently being employed to execute some tasks, such as monitoring of crops, identification of pests, maintenance of breeding grounds and greenhouses, soil analysis and application of pesticides, as in Schmale III et al. [2008] and Costa et al. [2012]. Figures 1.1(a), 1.1(b) and 1.2 show UAVs performing some of these tasks.

(a) Hexarotor (b) Fixed-wing

Figure 1.1 – (a) is hexarotor in a pulverization mission (Source: http://www.senar.org.br/agricultura-precisao/drone-aumenta-eficiencia-da-pulverizacao-agricola/), and (b) is a fixed-wing UAV in a monitoring mission (Source: www.santoslab.com).

Figure 1.2 – An MQ-9 Reaper remotely piloted aircraft assigned to the California Air National Guard's 163rd (Source: https://dod.defense.gov/News/Article/Article/1348274/air-force-drones-help-california-firefighters-combat-wildfires/).

Despite the use of UAVs to perform these tasks, other activities require the use of ground mobile robots, called Unmanned Ground Vehicles (UGVs). In some activities, the use of ground robots is required to obtain more precision, security and payload in execution. In the agricultural industry, for example, these UGVs are used in harvest and planting, pesticide application with precision for a specific plant (avoiding wastes and reducing costs), among others, enabling research as in Cheein and Carelli [2013] and Velasquez et al. [2016]. The UGVs are commonly used to load and people transportation, due to increased safety and load capacity in relation to UAVs, as in Jo et al. [2014] and Dias et al. [2015]. In addition, there are some locations of difficult operation for UAVs, such as caves and mines, requiring the use of ground robots. These conditions inspired the SubT DARPA challenge[1], where scientist teams from around the world are challenged to develop robots that is able to move, detect objects and map subsurface networks of caves and mines in unpredictable conditions. The Figures 1.3(a), 1.3(b), 1.4(a) and 1.4(b) shows UGVs performing some tasks autonomously.

(a) Autonomous Passenger Car (b) HX01 prototype

Figure 1.3 – (a) is an autonomous car developed by the UBER company (Source: https://www.b9.com.br/65014/uber-revela-seu-carro-autonomo/), and (b) is an autonomous loader vehicle (HX01) under developing by Volvo (Source: https://www.volvoce.com/deutschland/de-de/about-us/news/2016/elektrische-baustellenloesung/).

[1] www.subtchallenge.com

(a) Autonomous Passenger Car

(b) CMU prototype for the DARPA Challenge

Figure 1.4 – (a) is an autonomous tractor in an farming mission (Source: www.asirobots.com), and (b) is the robot developed by Carnegie Mellon University (CMU) for the SubT DARPA challenge.

These robots can be remotely operated by human pilots or autonomously guided by embedded navigation systems. Thus, to perform autonomous tasks with precision and efficiency, it is necessary a robust navigation system, which can often be expensive. In this context, this dissertation is motivated to develop a low-cost navigation system to control an UGV in tracking autonomously longitudinal trajectories.

1.2 Problem

In an autonomous system, it is important that the control system operates robustly and precisely during missions. In several scenarios of UGVs, discussed in the last section, the robot must travel across uneven and unstructured terrains, as in mining and agriculture tasks. These scenarios can directly affect the performance of an UGV in the execution of tasks at higher speeds.

Terrain irregularities and soil type can affect the speed dynamics of the robot, as well as changes in mass with the inclusion of extra loads in delivery tasks. These disturbances may cause serious control problems to ensure the robot's mobility. In Ferreira et al. [2018] a control system was developed to a UGV based on a kinematic model, which does not address these effects, and it was noted that in some terrains, the controller cannot follow the reference speeds.

This thesis is associated with the research project *"APIAR: robot development for crop inspection"* (APQ-03433-15 - Fundação de Amparo à Pesquisa do Estado de Minas Gerais (FAPEMIG)) which aims to build a four-wheeled electric robotic platform, to perform the task of exploring and collecting data from an area of agricultural cultivation. Therefore, the main problem to be addressed in this dissertation is the development of a small car-like UGV platform, equipped with sensors and a control system, that minimize the effects of adverse agricultural terrain conditions in a payload delivery task with longitudinal trajectories. These adverse conditions are associated with slopes on the ground, soil friction, and mass changes.

1.3 Related Works

This section presents some recent and important works related to trajectories tracking in UGVs and control strategies. Linked to extensive employment of mobile autonomous agents in several tasks, many papers concerning autonomous (or semi-autonomous) four-wheeled normal-size and small-size vehicles have been presented in the literature.

In Jo et al. [2015] an autonomous system is implemented in a distributed way for a passenger car. The system is composed by localization, perception, trajectory planning and vehicle control algorithms, which have been implemented to drive in a track that simulates daily traffic. The system must detect traffic lights, overtaking, school zone and sudden obstacle, among others.

Wit et al. [2004] presents a path tracking technique called "vector pursuit", which generates the desired vehicle turning radius based on the vehicle's current position and orientation, relative to the position of a point ahead on the planned path and the desired orientation along the path at that point. The authors performed experiments using a four-wheeled normal-size vehicle to analysis the performance, but only in lower speeds.

For small-size vehicles, Dos Santos et al. [2016] presents a simultaneous localization and mapping (SLAM) method for robot localization in monitoring tasks on vineyards. Robot localization is estimate by a sensor fusion. The method was validated by experiments in a small platform AGROB V14 equipped with a laser, camera, Inertial Measurement Unit (IMU), Global Positioning System (GPS) and an encoder.

Following agricultural applications, Ruiz-Larrea et al. [2016] presentes a four-wheeled UGV robot platform, equipped with infrared temperature and moisture sensors, for measuring the ground properties of the greenhouses. The Navigation system of the robot is composed by perception (with an extended Kalman filter), localization, path planning, and control systems. From real experiments, the data collected by temperature and humidity sensors in a controlled greenhouse is presented.

In addition, many other papers concerning modeling and control strategies have been proposed to address such platforms [Amer et al., 2017; Attia et al., 2014]. When addressing on-the-ground tasks, terrain conditions play an important rule on the robot's navigation, especially at higher speeds. Since most applications in outdoor scenarios occur under non-structured conditions, robust control techniques have been increasingly employed for a variety of robotic and automation tasks [Bahadorian et al., 2011; Bennis et al., 2008; Du et al., 2011].

1.3.1 UGV Control Strategies

The general problem of trajectory tracking for wheeled robots has a wide range of solutions. In Thanok and Parnichkun [2015] is presented a longitudinal control for a passenger car,

model *Mitsubishi Galant* produced in 1989. The car has been modified to perform autonomous tasks, equipped with on-board sensors such as Lidars and encoders. The model used is simplified, neglecting ground terms such as slopes and friction. The throttle control is by means of a Sliding Mode Control (SMC) approach, whereas the brake control relies on a Mamdani fuzzy controller. The SMC parameters were adjusted by a stochastic optimization technique, based on outdoor experiments on a plane pavement road.

In Cariou et al. [2009], the authors provide an adaptive and predictive control algorithm for an autonomous tractor, to executing straight line and curve path tracking on slippery and sloped terrains. Although considered road inclinations in the problem, only kinematic parameters are used in the model, making the strategy susceptible to dynamics issues. Similarly, in Kong et al. [2015], is presented a Model Predictive Control (MPC) to control an autonomous vehicle. In that paper, a kinematic model was used to design the control system and experiments show that at higher speeds the system is subject to dynamic issues that affect the performance of the controller.

An issue generally associated with predictive control is computational cost. Although robust, nonlinear and adaptive variations of MPC can properly address many challenges, on-board computers of robots must be relatively powerful to solve optimization problems at higher rates in real-time. Therefore, more expensive embedded computers with higher requirements of energy and payload must be employed.

Concerning more classical approaches, in Dias et al. [2015] the authors present model identification and speed control based on the longitudinal dynamics of car-like vehicles. Environment characteristics such as inclination, viscous friction, and aerodynamic resistance have also been considered, however, stability was ensured by two PI (proportional-integral) controllers, without robustness guarantees. In Foster et al. [2005], the Proportional-Integral-Derivative (PID) controller has been implemented for the velocity control of a windrow, an agricultural machine used for hay and forage preparation, crop harvesting, and crop residue processing. A first-order model with time delay was developed for the speed control, whose parameters were estimated by using a modified recursive-least-squares algorithm. The design follow a pole allocation for the nominal model, without robustness guarantees. In Oliveira et al. [2018], is presented the development of a small UGV platform for agricultural tasks. In the control system, a pure proportional controller based has been used in the velocity and orientation error. However, a kinematic model was used for the vehicle and the real experiments performed in a controlled ambient with a plane pavement, not validating for uneven terrain.

Some works can be found in the literature proposing the usage of the Linear Matrix Inequality (LMI) machinery to design controllers for trajectory tracking for car-like robots. In Alcala et al. [2018] a trajectory tracking is proposed using a Lyapunov control technique with a Linear Quadratic Regulator (LQR)-LMI tuning. The controller was tested in an Electric Tazzari Zero passenger car. However, a kinematic model was used for the vehicle and the experiments

performed on a plane pavement road, not checking the robustness to changes in the terrain.

It is possible to observe that many works in the literature present control strategies only based on kinematic parameters of the vehicles, leaving aside other important characteristics such as weight, friction and drag forces, and other terrain features.

1.3.2 Robust Control

As mentioned in the previous section, some parameters can have a considerable influence on the system. In this context, some papers relate to robust controllers to these influences. The authors of Gat et al. [2016] present a steering control algorithm for a car-like mobile robot connected to an overhead guide in greenhouse applications. A robust control law (at low speeds) was designed and the asymptotic stability verified and demonstrated with simulated and real-world experiments. However, assumptions such as constant and known ground slope and flat soil are not too realistic, even in enclosed places. The friction in the fork-to-rail connection was also disregarded, but its inclusion in the control design can be helpful to improve the results.

Kayacan et al. [2016] presents a robust trajectory tracking predictive control for UGVs. In this paper, a tractor-trailer system was modeled and controlled over linear and curvilinear target paths. Small tracking errors have been reported, but only experiments in kinematic "ideal" circumstances have been illustrated. Trailer's mass and friction would certainly be problems to be considered in more realistic scenarios.

A robust MPC have been proposed in Gray et al. [2013] in order to enforce safety constraints to control a semiautonomous UGV to follow a path, avoiding obstacles. Uncertainties have been added to the input of the model and robust control laws designed to compute the smallest corrective steering action to keep the drive safe in the trajectories. Despite considering uncertainties in the model, it were performed only simulated results.

In Du et al. [2011] a robust controller design by an LMI approach is proposed to control the yaw moment of a vehicle, considering uncertainties in the cornering stiffness and tire-road conditions. The state feedback controller have been designed by solving LMIs to obtain the gain matrix to stabilization. Despite the good results, only simulated experiments were performed. In addition, the full state feedback control method requires measurement of all states, making a practical project more complex and expensive.

1.3.3 Backstepping Control

In Low and Wang [2005] a Backstepping robust controller is presented to control an *Ackerman* vehicle. The robust design treats the longitudinal speed in a kinematics model. Despite treating the longitudinal speed uncertainty, only simulations experiments is presented with a kinematics model, not investigating the dynamic effects influenced by the terrain.

A variant of a SMC that combines backstepping and fuzzy sliding mode controller is adopted in Wu et al. [2019], for the speed control of a differential platform. The robot developed by the authors was tested indoors, navigating on a smooth flat surface. Although adaptive/intelligent controllers may promise a robust solution, the process of designing and developing each controller can be time-consuming and specific for each application [Amer et al., 2017, Sec. 3.4].

In Salierno and Raffo [2017] it is proposed a controller to a quadrotor UAV with six degrees of freedom dynamics (6DOF). The presented control law is based in the backstepping method with an integral action, to guarantee convergence for a time-varying trajectory reference. The controller is based on full state feedback that controls all 6DOF freedom degree, translation and orientation. Simulated results shown the controller performance and the improvements of integral action.

Fang and Gao [2011] presents an adaptive method to robustify a backstepping design. The authors use a backstepping with integral action to control attitude, altitude and horizontal position of a quadrotor UAV with a 6DOF freedom degree model. The adaptive design is for compensate model uncertainties, but the estimation of this disturbance is online, increasing computational and implementation costs. Simulated results for small variations in the mass of the robot and including external disturbances are shown.

In Zhou and Liu [2010], a cascade control, based on a sliding-mode and backstepping approach to control the tire yaw of a vehicle, was proposed. It was considered that the longitudinal forces acting on the vehicle are unknown disturbances and the control law calculated step by step using backstepping and sliding-mode approach. The analysis of the controller performance is based on simulated experiments, but changes in the terrain were not considered.

1.4 Objectives

The main goal of this work is to solve a longitudinal trajectory tracking problem of UGVs in adverse situations, considering a dynamic model with the influence of external disturbances and uncertain parameters.

The specific objectives are:

1 Design a PID controller to perform a longitudinal trajectory tracking and to be robust to uncertain parameters and external disturbances, using an LMI approach;

2 Design an Integral Backstepping nonlinear control to perform a longitudinal trajectory tracking, minimizing the influence of disturbances;

3 Develop a real UGV platform that allows doing tasks in irregular terrains, following a longitudinal trajectory, using the developed controllers;

4 Compare the control strategies in simulated and real-world experiments, evaluating their performances.

1.5 Publications

This dissertation contributed to the following publications:

- [Ferreira et al., 2018] Ferreira, E., Miranda, V.R.F.; Silva Junior, M., Mozelli, L. A., Alves Neto, A. Aplicação de plataforma android no controle de robôs móveis para inspeção de lavouras. Congresso Brasileiro de Automática - CBA 2018. João Pessoa - PB.
  - This paper proposed an embedded navigation system to control UGVs, using an *Android smartphone*. The control system operates on the smartphone and, using an application, it was possible to define a set of *waypoints* that should be visited by the robot. The controllers were based on a kinematic model of the robot and, using the GPS and IMU data provided by the smartphone, it was possible to control their position, orientation and speed. This was the first prototype of this work, being adopted for the purposes of modeling and concept proof.

- [Miranda et al., 2018] Miranda, V.R.F., Alves Neto, A., Mozelli, L.A. Estudo sobre estratégias de controle longitudinal para robôs terrestres em terrenos irregulares com inclinação. Congresso Brasileiro de Automática - CBA 2018. João Pessoa - PB.
  - In this paper, it was proposed the model of the longitudinal dynamics of a car-like UGV, considering the irregularities and inclinations in off-road terrains. The objective was to control this system to track longitudinal trajectories in a payload delivery task in agricultural environments. Therefore, two methodologies are employed: a robust PID controller, tuned by an LMI approach, and a non-linear Backstepping controller. To the robust PID tuning, parametric uncertainties have been considered in the system, related to the uneven terrain and the changing in the mass. Simulation results were made to compare both techniques performances.

Others publications accepted for publication:

- Miranda, V.R.F., Alves Neto, A., Mozelli, L.A. Longitudinal Trajectory Tracking for UGVs on Agricultural Terrains. Simpósio Brasileiro de Automação Inteligente - SBAI 2019.
  - This paper presents the development of a low cost small car-like semi-autonomous vehicle platform (Fig. 1.5) to perform tasks in agricultural terrains. Based on the nonlinear dynamics of such vehicles, a *Backstepping* controller with an integral

part was developed to execute these tasks in longitudinal trajectories. Real-world experiments were present comparing the performance of the controller developed in this paper with the others in Miranda et al. [2018].

In addition, it contributed to the development of a semi-autonomous UGV platform for experiments in irregular terrains (Fig. 1.5).

Figure 1.5 – Simulation results of Table 4.4: position and speed trajectory.

1.6 Dissertation Structure

The dissertation is structured as follows: Chapter 2 present a literature review of techniques used in the strategy to control the robot; Chapter 3 formalizes the approached problem with the modeling of vehicle longitudinal dynamics and the design of control strategies proposed; In Chapter 4 are presented simulation and real-world experiments to validate the strategies used, as well as a description of the platform developed to the experiments; Finally, Chapter 5 offers the conclusion and future perspectives of the research.

CHAPTER

2

PRELIMINARY CONCEPTS

This chapter is dedicated to a literature review about the control techniques employed throughout this dissertation and some concepts associated with them.

2.1 Lyapunov Stability

Stability of linear systems in state space form is usually associated with the eigenvalues of the coefficient matrix or, in case of transfer functions, associated with the location of the poles [Chen, 1998]. This analysis can be generalized to nonlinear systems by the Lyapunov Stability Theory.

The state-space description models a dynamic system by means of a set of coupled first-order differential equations. Each equation is related to an internal variable, called state variable. The concept of state of a system refers to the minimum set of variables that fully describe the system and its response to external variables, the input variables. This set of variables is not unique, but the number of state variables n must remain the same, nonetheless. The scalar n is called the order of a systems. Alternatively, the state-space can be regarded as an Euclidean space, of dimension n, whose coordinates are the state variables, a state is a given vector within this space and the system dynamic is represented by a vector field.

Following the theory in Krstic et al. [1995] and Khalil and Grizzle [2002], consider an autonomous[2] system, devoided of inputs:

$$\dot{x} = \mathbf{f}(x), \tag{2.1}$$

where f is piecewise continuous in t, locally Lipschitz in $x \in \mathbb{R}^n$ and $x = 0$ is an equilibrium point. The function f is stable in the Lyapunov sense at the origin if for a candidate function (Lyapunov

[2] In this thesis, autonomous system is regarded as a dynamic system described by ordinary differential equation which does not explicitly depend on the independent variable. When this variable is time, it can be also called a time-invariant system.

function), continuously differentiable, $\mathbf{V} : \mathbf{D} \to R^n$, such that $\mathbf{D}$ is a domain containing $x = 0$,

$$\mathbf{V}(0) = 0,\ \mathbf{V}(x) > 0 \text{ in } \mathbf{D} - \{0\}, \tag{2.2}$$

$$\dot{\mathbf{V}}(x) \leq 0 \text{ in } \mathbf{D}. \tag{2.3}$$

Also, (2.1) is asymptotically stable in the origin if

$$\dot{\mathbf{V}}(x) < 0 \text{ in } \mathbf{D} - \{0\}, \tag{2.4}$$

and globally asymptotically stable if

$$\mathbf{V}(0) = 0,\ \mathbf{V}(x) > 0,\ \forall x \neq 0, \tag{2.5}$$

$$||x|| \to \infty \Rightarrow \mathbf{V}(x) \to \infty, \tag{2.6}$$

$$\dot{\mathbf{V}}(x) < 0,\ \forall x \neq 0. \tag{2.7}$$

In the case of time-varying systems, piecewise continuous in t and locally Lipschitz in x, as

$$\dot{x} = f(t,x), \tag{2.8}$$

it will be uniformly stable in the Lyapunov sense at the origin if for a candidate continuously differentiable function $\mathbf{V} : [0,\infty]x\mathbf{D} \to R^n$, such that $\mathbf{D}$ is a domain containing $x = 0$ and

$$\mathbf{W}_1(x) \leq \mathbf{V}(t,x) \leq \mathbf{W}_2(x), \tag{2.9}$$

$$\frac{\partial \mathbf{V}}{\partial t} + \frac{\partial \mathbf{V}}{\partial x} f(t,x) \leq 0,\ \forall t \geq 0 \text{ and } \forall x \in \mathbf{D}, \tag{2.10}$$

where $\mathbf{W}_1(x)$ and $\mathbf{W}_2(x)$ are continuous positive definite on $\mathbf{D}$.

As in autonomous case, it can be extended to a uniformly asymptotically stable if the assumptions (2.9), (2.10) and (2.11) are satisfied, for a $\mathbf{W}_3(x)$ continuous positive definite on $\mathbf{D}$. Moreover, the system (2.8) is globally uniformly asymptotically stable if the same conditions are satisfied with a radially unbounded $\mathbf{V}(t,x)$.

$$\frac{\partial \mathbf{V}}{\partial t} + \frac{\partial \mathbf{V}}{\partial x} f(t,x) \leq -\mathbf{W}_3(x),\ \forall t \geq 0 \text{ and } \forall x \in \mathbf{D} \tag{2.11}$$

In a linear case, the system is asymptotically stable by root locus analysis if it poles are in the left half plane or if all real parts of eigenvalues of the coefficient matrix are less than zero, that is, if the system is Hurwitz. This can be investigated by the following Lyapunov's method, as in Chen [1998] and Khalil and Grizzle [2002]. Consider the system:

$$\dot{\vec{x}} = \mathbf{A}\vec{x}, \tag{2.12}$$

and the quadratic Lyapunov function candidate

$$\mathbf{V}(x) = \vec{x}^T \mathbf{P} \vec{x}, \tag{2.13}$$

where $\mathbf{P} = \mathbf{P}^T$. From the Lyapunov theory, the system is asymptotically stable if $\mathbf{V}(x) > 0$ and $\dot{\mathbf{V}}(x) < 0$, then

$$\mathbf{V}(x) = \vec{x}^T \mathbf{P} \vec{x} > 0 \rightarrow \mathbf{P} > 0, \forall \vec{x} \neq 0 \tag{2.14}$$

and

$$\dot{\mathbf{V}}(x) = \vec{x}^T \mathbf{P} \dot{\vec{x}} + \dot{\vec{x}}^T \mathbf{P} \vec{x} < 0 \tag{2.15}$$

$$\dot{\mathbf{V}}(x) = \vec{x}^T (\mathbf{PA} + \mathbf{A}^T \mathbf{P}) \vec{x} < 0 \tag{2.16}$$

$$\mathbf{PA} + \mathbf{A}^T \mathbf{P} < 0 \tag{2.17}$$

This particular inequality can be solved as a linear equation if exist a $\mathbf{Q} = \mathbf{Q}^T > 0$ such that

$$\mathbf{PA} + \mathbf{A}^T \mathbf{P} = -\mathbf{Q}, \tag{2.18}$$

$$\mathbf{PA} + \mathbf{A}^T \mathbf{P} + \mathbf{Q} = 0. \tag{2.19}$$

2.1.1 Control Lyapunov Function

In control design, Control Lyapunov Function (CLF) are regarded as an extension of the Lyapunov function to stability analysis of systems with control inputs. Following the CLF formulation in Krstic et al. [1995], consider the system

$$\dot{\vec{x}} = \mathbf{f}(\vec{x}, u), \;\; \vec{x} \in \mathbf{R}^n, \;\; u \in \mathbf{R}, \;\; f(0,0) = 0, \tag{2.20}$$

and a Lyapunov function $\mathbf{V}(x)$ smooth, positive definite and radially unbounded. This Lyapunov function will be a CLF for (2.20) if there is a control law u and $\mathbf{W}(x) > 0$ such that

$$\frac{\partial \mathbf{V}}{\partial \vec{x}} f(\vec{x}, u) \leq -\mathbf{W}(x) < 0, \;\; \forall \vec{x} \in \mathbf{R}^n \tag{2.21}$$

According to Krstic et al. [1995], the existence of a CLF for a given u in (2.20) is a necessary and sufficient condition for the global asymptotic stability of the system.

In case of a system affine in the control,

$$\dot{\vec{x}} = \mathbf{f}(\vec{x}) + \mathbf{g}(x)u, \;\; \mathbf{f}(0) = 0, \tag{2.22}$$

the inequality (2.21) becomes

$$\frac{\partial \mathbf{V}}{\partial \vec{x}} \mathbf{f}(\vec{x}) + \frac{\partial \mathbf{V}}{\partial \vec{x}} \mathbf{g}(\vec{x}) u \leq -\mathbf{W}(x) < 0. \tag{2.23}$$

2.2 Robust Control

Systems can be represented by an equation or a set of them. In dynamic systems, these equations carry information about the behavior of these systems over time. However, it is very difficult to obtain a set of equations that includes the true physical [Zhou and Doyle, 1998].

The equations that model the system are essential for analysis and control design. However, even with a model that is faithful to the behavior of the system, in some situations, the system parameters embedded in the equations may change with time, or it is not possible to determine them correctly. This uncertainty in the parameters can affect the performance of the controller, which has been tuned to a model with fixed parameters.

In feedback control, the main goal is to maintain the overall stability and system performance despite uncertainties in the plant. A controller designed for a nominal process model generally works fine for the nominal plant model but may fail for even a nearby plant model.

Robust control deals with this imperfectly process model and aims at designing a fixed (non-adaptive) controller such that some defined level of performance of the controlled system is guaranteed, irrespective of changes in plant dynamics within a predefined class [Herzog and Keller, 2011].

In control systems, these uncertainties in the models are classified into two categories: disturbance signals, caused by external stochastic inputs which are not under control (noises in the sensors and actuators), and perturbations in the plant dynamics, caused by changes in the plant parameters and unmodeled dynamics.

There are some robust control techniques that include these uncertainties into the controller design. To achieve this, it is necessary to have a mathematical description of model uncertainty. In the case of a time-invariant external disturbance, for example, which can be represented as a transfer function $\triangle(s)$, it is commonly included this disturbance as shown in Fig. 2.1, where $\triangle(s)$ is an additive perturbation of the nominal plant $G_0(s)$ and

$$G(s) = G_0(s) + \triangle(s) \tag{2.24}$$

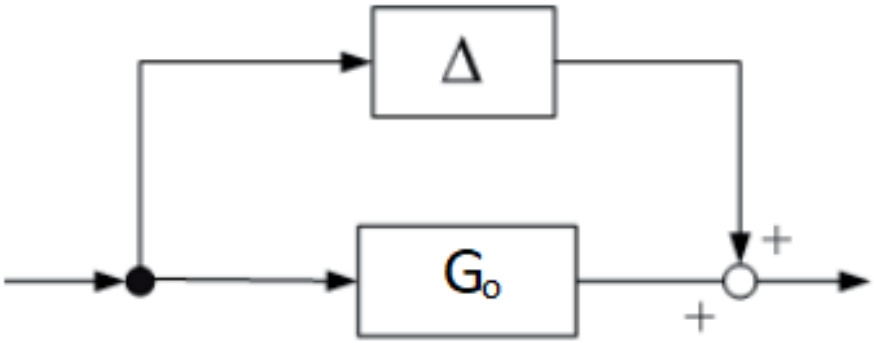

Figure 2.1 – Additive uncertainty

In the case of perturbations in the plant dynamics, that is, uncertain parameters in the model, it is commonly represent the system as a polytope in state space. Consider the uncertain

linear system:

$$\dot{\vec{x}} = \mathbf{A}(\alpha)\vec{x}, \tag{2.25}$$

where $A(\alpha)$ is a coefficient matrix with uncertainty, and

$$\mathbf{A}(\alpha) \in \mathscr{A},$$

where $\mathscr{A}$ is a polytope describe as:

$$\mathscr{A} = \left\{ \mathbf{A}(\alpha) \ : \ \mathbf{A}(\alpha) = \sum_{i=1}^{N} \alpha_i \mathbf{A}_i; \ \sum_{i=1}^{N} \alpha_i = 1; \ \alpha_i \geq 0 \right\}, \tag{2.26}$$

where $\mathbf{A}_i$ are known vertices formed by N extreme values (maximum and minimum) of k uncertainties, with $N = 2^k$.

There are some feedback control methods that address these problems. Some of them use an output feedback approach, while others use state feedback. The following section compares these approaches.

2.3 Output Feedback and State Feedback

The states of a system are variables that describe the behavior of the system. In the control design, the deal is positioning the system closed-loop eigenvalues in the desired location, where, in most cases, it is chosen to make the system stable. This is usually done with the feedback of the states.

In a full state feedback controller, it is possible to control the system by using the information of all variables that influence it. Even if the objective is to control just one interest variable, the possibility of collect information from all states of the system gives us greater control over the behavior of all system.

Consider a linear system, the state feedback control law can be describes as in Fig. 2.2 and by the following equation [Chen, 1998; Franklin et al., 2014]:

$$\vec{u} = -\mathbf{K}\vec{x}, \tag{2.27}$$

where $\vec{u}$ is the input vector, $\vec{x}$ the measured states vector and $\mathbf{K}$ the control gain.

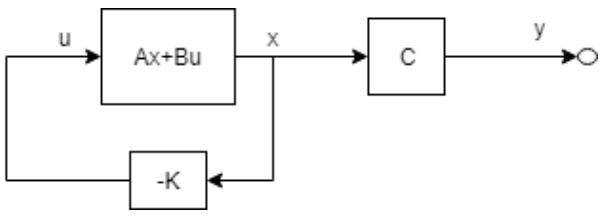

Figure 2.2 – State Feedback

At many times, despite having a model that satisfactorily describes the dynamics that influence a system, it is not always possible to measure (collect information) a particular state in practice. In this case, where the interest state can be measured and other states cannot, the output feedback controller can be an alternative.

The output feedback control law can be described as in Fig. 2.3 and by the following equation

$$\vec{u} = -\mathbf{K}\vec{y}, \tag{2.28}$$

where $\vec{u}$ is the input vector, $\vec{y}$ the measured output and $\mathbf{K}$ the control gain.

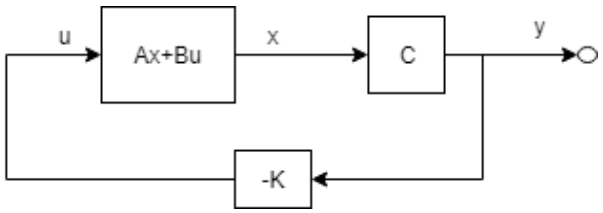

Figure 2.3 – Output Feedback

With output feedback there is no need to measure all states of the system to design a feedback controller, which can be an advantage. Another advantage is the low cost in practical implementations, due to the number of sensors needed. However, the state feedback, generally, has a better performance controlling all the variables that affect the system.

Another case occurs when the interest state cannot be measured. In this case, it may possibly use a state observer to estimate the state value. This methodology will not be addressed in this text and can be seen in Franklin et al. [2014] and Chen [1998].

2.4 Linear Control

A system is called linear if the superposition property holds and nonlinear if does not [Chen, 1998]. The mathematical model is one of the main ways to represent the behavior of a system, be it linear or nonlinear.

The nonlinearities in the systems can be represented in their mathematical nonlinear model. Sometimes, it is difficult analyzing nonlinear models. Therefore, linearization techniques were developed that make it possible to approximate a nonlinear model of a system to a linear representation, as in Chen [1998].

From these linear mathematical representations for systems, several controller's design methods have appeared over the years. The goal is to design a system to control the behavior of another system based on their mathematical model.

This section presents linear control methods that will be addressed throughout the dissertation.

2.4.1 Proportional-Integral-Derivative (PID) Controller

The PID controller is one of the most popular controllers in the industrial sector. Despite being an almost centenary method, its simplicity made it present in more than 90% of process control applications, as we can see in Mozelli and Souza [2016]. This controller is based on three-terms tuning, and has the following transfer function in the parallel form:

$$C(s) = K_p + K_i\frac{1}{s} + K_d s, \tag{2.29}$$

where $K_p,\ K_i,\ K_d$, represent the proportional, integral and derivative gains, respectively.

Since the first PID controller tuning proposal to these gains was made by Ziegler and Nichols [Ziegler and Nichols, 1942], several works were developed over the years to propose other tuning methods, including works such as in Ang et al. [2005], Li and Li [2011] and Zhang and Furusho [2000].

The PID controller is a technique more suitable to linear models, due to the tuning methods used. Since non-linear dynamics are ubiquitous, approximation techniques to devise a linear model are suitable for a control design.

2.4.2 Linear Matrix Inequalities (LMI)

According Boyd et al. [1994] and Mozelli [2008], an Linear Matrix Inequality (LMI) has the form:

$$\mathbf{F}(x) = \mathbf{F}_0 + \sum_{i=1}^{m} \vec{x}_i \mathbf{F}_i > 0, \tag{2.30}$$

where $\vec{x} \in \mathbf{R}^m$ is the variable and the $\mathbf{F}_i = \mathbf{F}_i^T \in \mathbf{R}^{nxn},\ i = 0,...,m$, are given.

There is no distinction between a set of LMIs and a single LMI, that is, a set of LMIs can be represented by a single LMI:

$$\mathbf{diag}\{\mathbf{F}^{(1)}(x),...,\mathbf{F}^{(p)}(x)\} > 0 := \{\mathbf{F}^{(1)}(x) > 0,...,\mathbf{F}^{(p)}(x) > 0\} \tag{2.31}$$

Some nonlinear inequalities can be converted to an LMI form using Schur complements. According Zhang [2006] and Boyd et al. [1994], let $\mathbf{Q}(x) = \mathbf{Q}(x)^T, \mathbf{R}(x) = \mathbf{R}(x)^T > 0, \mathbf{S}(x)$, the inequality

$$\mathbf{Q}(x) - \mathbf{S}(x)\mathbf{R}^{-1}(x)\mathbf{S}^T(x) > 0, \tag{2.32}$$

is equivalent to

$$\begin{bmatrix} \mathbf{Q}(x) & \mathbf{S}(x) \\ \mathbf{S}^T(x) & \mathbf{R}(x) \end{bmatrix} > 0. \tag{2.33}$$

In particular, linear inequalities, convex quadratic matrix inequalities, matrix norm inequalities, and constraints that arise in control theory, such as in Lyapunov, can all be described

in the form of an LMI. Therefore, the inequality (2.17) from the Lyapunov Stability theory in the section 2.1 is equivalent to an LMI.

The LMI problems are normally solved as a convex optimization problem, using numerical solvers with the LMIs constraints. The system stability can be analyzed by solving an LMI problem. Consider an uncertain system at (2.25), as in Boyd et al. [1994] and Zhou and Doyle [1998], the necessary and sufficient conditions to check the stability of the system (2.25) are:

- The vertices of $\mathbf{A}(\alpha)$ need to be stable;
- There is a $\mathbf{P} = \mathbf{P}^T > 0$, such that the following LMIs are satisfied:

$$\mathbf{P}\mathbf{A}(\alpha) + \mathbf{A}(\alpha)^T\mathbf{P} < 0, \tag{2.34}$$

$$\mathbf{P}\mathbf{A}_i + \mathbf{A}_i^T\mathbf{P} < 0,\ i = 1,...,N. \tag{2.35}$$

This is a Robust control problem (model uncertainties) that can be solved using *MATLAB* optimization solvers as SeDumi [Sturm, 1999] and Mosek [Mosek, 2015] with a package that make an interface to the LMI problem, as the Yalmip [Löfberg, 2004]. The next sections presents some control problems that can be solved by an LMI approach.

2.4.3 Static Output Feedback (SOF) Control using LMIs

The Static Output Feedback (SOF) is a control method commonly used in problems where is not necessary measure all states or when it is not possible to get information about all the states present in the model (section 2.3). In this method, the input of the system is given by the control law

$$\vec{u}(t) = -\mathbf{K}\vec{y}(t), \tag{2.36}$$

where $\vec{u}(t)$ is the inputs vector, $\vec{y}(t)$ the outputs vector and $\mathbf{K}$ is the control gains matrix.

The goal is to find $\mathbf{K}$ that stabilize the system. One way to do this is by using the Lyapunov's stability theory by LMIs, as in Cao et al. [1998]. Consider the system

$$\begin{aligned} \dot{\vec{x}}(t) &= \mathbf{A}\vec{x}(t) + \mathbf{B}\vec{u}(t) \\ \vec{y}(t) &= \mathbf{C}\vec{x}(t), \end{aligned} \tag{2.37}$$

using the SOF control law in the closed loop and rewriting, we have

$$\dot{\vec{x}}(t) = \mathbf{A}_f\vec{x}(t),\ \ \mathbf{A}_f = (\mathbf{A} - \mathbf{B}\mathbf{K}\mathbf{C}). \tag{2.38}$$

Based on the theory described in sections 2.1 and 2.4.2, for the closed-loop system (2.38) be considered stable, the follow inequalities must to be satisfied for a $\mathbf{P} = \mathbf{P}^T > 0$:

$$\mathbf{P}\mathbf{A}_f + \mathbf{A}_f^T\mathbf{P} < 0, \tag{2.39}$$

$$\mathbf{P}(\mathbf{A} - \mathbf{B}\mathbf{K}\mathbf{C}) + (\mathbf{A} - \mathbf{B}\mathbf{K}\mathbf{C})^T\mathbf{P} < 0, \tag{2.40}$$

$$\mathbf{P}\mathbf{A} + \mathbf{A}^T\mathbf{P} - \mathbf{P}\mathbf{B}\mathbf{K}\mathbf{C} - \mathbf{C}^T\mathbf{K}^T\mathbf{B}^T\mathbf{P} < 0. \tag{2.41}$$

The inequality (2.41) is not an LMI and just by using the Schur complement is not possible to convert to a LMI problem. These inequalities are called Bilinear Matrix Inequalities (BMIs), which is a non-convex problem due to the nonlinearities involving the variable matrix $\mathbf{P}$ and $\mathbf{K}$ [VanAntwerp and Braatz, 2000]. In case of the matrix $\mathbf{B}$ (or $\mathbf{C}$) is square and invertible, this problem can be transformed to an LMI problem by variable changes as follows:

$$\mathbf{PA} + \mathbf{A}^T\mathbf{P} - \mathbf{LC} - \mathbf{C}^T\mathbf{L}^T < 0, \tag{2.42}$$

where $\mathbf{L} = \mathbf{PBK}$ and $\mathbf{K} = (\mathbf{PB})^{-1}\mathbf{L}$.

However, in cases which it is not possible to make these changes, it is necessary a new method to solve problems like this. Some methods are commonly used to solve BMIs problems, an example is finding an initial matrix $\mathbf{P} = \mathbf{P}^T > 0$ such that the system is stable in open loop and then use this to find the matrix $\mathbf{K}$ that stabilize in the closed loop. Some papers as Cao et al. [1998] and He and Wang [2006] proposed methods in this sense, which will be addressed over of this dissertation.

2.4.4 Static Output Feedback (SOF) $\mathscr{H}\infty$ Control using LMIs

The $\mathscr{H}\infty$ system norm represents the highest energy gain of a system can offer to a noise input signal, that is, how much a noise signal can affect the system. The $\mathscr{H}\infty$ based control project is an optimization problem such that it is intended to minimize this gain effect in external noisy signals by a closed loop control law, robustifying the system (section 2.2).

Consider the system

$$\begin{aligned} \dot{\vec{x}}(t) &= \mathbf{A}\vec{x}(t) + \mathbf{B}_w\vec{w}(t) \\ \vec{z}(t) &= \mathbf{C}_z\vec{x}(t) + \mathbf{D}_{wz}\vec{w}(t),\ \vec{x}(0) = 0,\ \vec{x}(\infty) = 0, \end{aligned} \tag{2.43}$$

where $\vec{x}(t) \in \mathbf{R}^n$ is the states vector, $\vec{w}(t) \in \mathbf{R}^{n_w}$ the input noise vector, $\vec{z}(t) \in \mathbf{R}^{n_z}$ the outputs, and $\mathbf{A}, \mathbf{B}_w, \mathbf{C}_z, \mathbf{D}_{wz}$ with appropriate dimensions. In a frequency domain representation:

$$\mathbf{H}_{wz}(s) = \mathbf{C}_z(s\mathbf{I} - \mathbf{A})^{-1}\mathbf{B}_w + \mathbf{D}_{wz}. \tag{2.44}$$

The $\mathscr{H}\infty$ norm of (2.43) is

$$||\mathbf{H}_{wz}(s)||_\infty = max_w|\mathbf{H}(jw)|, \tag{2.45}$$

and, according Zhou et al. [1996] and Chang [2014], can be represented by

$$\int_0^\infty \vec{z}^T(t)\vec{z}(t)dt < \gamma^2 \int_0^\infty \vec{w}^T(t)\vec{w}(t)dt, \tag{2.46}$$

where γ is an upper limit to the norm. The norm value can be obtained by a convex optimization problem to minimize γ, that is, can be treated as an LMI problem. From the Lyapunov's function $\mathbf{V}(x) = \vec{x}^T(t)\mathbf{P}\vec{x}(t)$, such that $\mathbf{P} = \mathbf{P}^T > 0$ and

$$\dot{\mathbf{V}}(x) + \vec{z}^T(t)\vec{z}(t) - \gamma^2\vec{w}^T(t)\vec{w}(t) < 0, \tag{2.47}$$

following the *Bounded Real Lemma* [Boyd et al., 1994; Chang, 2014; Zhou et al., 1996]:

$$\dot{\mathbf{V}}(x)+\vec{z}^T(t)\vec{z}(t)-\gamma^2\vec{w}^T(t)\vec{w}(t)=\begin{bmatrix}\vec{x}\\ \vec{w}\end{bmatrix}^T\begin{bmatrix}\mathbf{A}^T\mathbf{P}+\mathbf{P}\mathbf{A}+\mathbf{C}_z^T\mathbf{C}_z & \mathbf{P}\mathbf{B}_w+\mathbf{C}_z^T\mathbf{D}_{wz}\\ \mathbf{B}_w^T\mathbf{P}+\mathbf{D}_{wz}^T\mathbf{C}_z & -\gamma^2\mathbf{I}+\mathbf{D}_{wz}^T\mathbf{D}_{wz}\end{bmatrix}\begin{bmatrix}\vec{x}\\ \vec{w}\end{bmatrix}<0, \tag{2.48}$$

that results in solve

$$min\ \gamma^2:\begin{cases}\mathbf{P}>0,\\ \begin{bmatrix}\mathbf{A}^T\mathbf{P}+\mathbf{P}\mathbf{A}+\mathbf{C}_z^T\mathbf{C}_z & \mathbf{P}\mathbf{B}_w+\mathbf{C}_z^T\mathbf{D}_{wz}\\ \mathbf{B}_w^T\mathbf{P}+\mathbf{D}_{wz}^T\mathbf{C}_z & -\gamma^2\mathbf{I}+\mathbf{D}_{wz}^T\mathbf{D}_{wz}\end{bmatrix}<0,\end{cases} \tag{2.49}$$

that can be rewritten using Schur complement as

$$min\ \gamma:\begin{cases}\mathbf{P}>0,\\ \begin{bmatrix}\mathbf{A}^T\mathbf{P}+\mathbf{P}\mathbf{A} & \mathbf{P}\mathbf{B}_w+\mathbf{C}_z^T\mathbf{D}_{wz} & \mathbf{C}_z^T\\ \mathbf{B}_w^T\mathbf{P}+\mathbf{D}_{wz}^T\mathbf{C}_z & -\gamma\mathbf{I} & \mathbf{D}_{wz}^T\\ \mathbf{C}_z & \mathbf{D}_{wz} & -\gamma\mathbf{I}\end{bmatrix}<0.\end{cases} \tag{2.50}$$

Now, considering the following system

$$\begin{aligned}\dot{\vec{x}}(t)&=\mathbf{A}\vec{x}(t)+\mathbf{B}_u\vec{u}(t)+\mathbf{B}_w\vec{w}(t)\\ \vec{y}(t)&=\mathbf{C}_y\vec{x}(t)+\mathbf{D}_{wy}\vec{w}(t)\\ \vec{z}(t)&=\mathbf{C}_z\vec{x}(t)+\mathbf{D}_{uz}\vec{u}(t)+\mathbf{D}_{wz}\vec{w}(t),\end{aligned} \tag{2.51}$$

where $\vec{x}(t)\in\mathbf{R}^n$ is the state vector, $\vec{u}(t)\in\mathbf{R}^{n_u}$ is the input vector, $\vec{w}(t)\in\mathbf{R}^{n_w}$ the external input noise vector, $\vec{y}(t)\in\mathbf{R}^{n_y}$ the measured outputs, $\vec{z}(t)\in\mathbf{R}^{n_z}$ is an computed output, and $\mathbf{A},\mathbf{B}_w,\mathbf{B}_u,\mathbf{C}_z,\mathbf{C}_y,\mathbf{D}_{uz},\mathbf{D}_{wz},\mathbf{D}_{wy}$ with appropriate dimensions. According Chang [2014] and Zhou et al. [1996], in an SOF $\mathscr{H}\infty$ control design, the objective is to find an asymptotically stable SOF controller, such that the following conditions are satisfied for the system (2.51) with the control law $\vec{u}(t)=\mathbf{K}\vec{y}(t)$:

1 - The closed-loop system (2.52) is asymptotically stable when $\vec{w}(t)=0$;

2 - Under the zero initial condition, (2.46) is satisfied for any nonzero $\vec{w}(t)\in\mathscr{L}_2[0,\infty)$.

$$\begin{aligned}\dot{\vec{x}}(t)&=(\mathbf{A}+\mathbf{B}_u\mathbf{K}\mathbf{C}_y)\vec{x}(t)+(\mathbf{B}_w+\mathbf{B}_u\mathbf{K}\mathbf{D}_{wy})\vec{w}(t)\\ \vec{y}(t)&=\mathbf{C}_y\vec{x}(t)+\mathbf{D}_{wy}\vec{w}(t)\\ \vec{z}(t)&=(\mathbf{C}_z+\mathbf{D}_{uz}\mathbf{K}\mathbf{C}_y)\vec{x}(t)+(\mathbf{D}_{wz}+\mathbf{D}_{uz}\mathbf{K}\mathbf{D}_{wy})\vec{w}(t),\end{aligned} \tag{2.52}$$

Following the same approach seen earlier, these are sufficient conditions to satisfy the LMI problem (2.50) for the closed loop (2.52). Therefore, the tuning of $\mathbf{K}$ in an SOF $\mathscr{H}\infty$ control problem is obtained by solving the following BMI problem using an iterative method as was

proposed by Cao et al. [1998], He and Wang [2006] and Chaibet et al. [2005]:

$$min\ \gamma : \begin{cases} \mathbf{P} > 0, \\ \begin{bmatrix} \mathbf{A}_{cl}^T\mathbf{P} + \mathbf{P}\mathbf{A}_{cl} & \mathbf{P}\mathbf{B}_{cl} & \mathbf{C}_{cl}^T \\ \mathbf{B}_{cl}^T\mathbf{P} & -\gamma\mathbf{I} & \mathbf{D}_{cl}^T \\ \mathbf{C}_{cl} & \mathbf{D}_{cl} & -\gamma\mathbf{I} \end{bmatrix} < 0, \end{cases} \tag{2.53}$$

where

$$\begin{aligned} \mathbf{A}_{cl} &= \mathbf{A} + \mathbf{B}_u\mathbf{K}\mathbf{C}_y, \\ \mathbf{B}_{cl} &= \mathbf{B}_w + \mathbf{B}_u\mathbf{K}\mathbf{D}_{wy}, \\ \mathbf{C}_{cl} &= \mathbf{C}_z + \mathbf{D}_{uz}\mathbf{K}\mathbf{C}_y, \\ \mathbf{D}_{cl} &= \mathbf{D}_{wz} + \mathbf{D}_{uz}\mathbf{K}\mathbf{D}_{wy}. \end{aligned}$$

This control method can be extended to a robust SOF $\mathscr{H}\infty$ controller when assuming a system with model uncertainties. The procedures are the same as demonstrated in the previous section, but using the BMI problem (2.53).

2.5 Nonlinear Control

Most systems present in nature have nonlinearities which often have a influence on their behavior. Control methodologies have been arisen over time in order to control these systems. Mathematical models take into consideration these nonlinearities and are the basis of the control projects.

Next subsections presents a classical nonlinear control method called Backstepping.

2.5.1 Standard Backstepping

In this section, we will describe the Backstepping control technique for nonlinear systems. This technique is an approach to stabilize the origin of systems by a full states feedback control law design based on the Lyapunov Stability Theory (section 2.1).

As seen in Khalil and Grizzle [2002] and Krstic et al. [1995], this methodology uses virtual control inputs as the feedback control laws to stabilize subsystems obtained from the objective system. These virtual control laws are inserted to the subsystems by the change of variables between the original states of the system. These stabilizing virtual control laws are selected step by step for each subsystem seeking stability in a recursively form until the last subsystem, where the control law of the objective system begins to act, determining a stabilizing control law for the original system.

This controller design method can be advantageous because of the simplification in the analysis of high order systems by reducing them to smaller subsystems and, finally, obtaining a stabilizing control law for the original system.

The design flexibility of the method, due to its recursive use of the Lyapunov Function, it is an advantage with respect to other nonlinear methods. This flexibility makes the method less restrictive than others. For example, relaxing the matching condition imposed as in the SMC [Khalil and Grizzle, 2002].

In theory, the Backstepping method can compensate exactly the uncertainties present in the state variables. However, it is not always necessary to cancel all nonlinear dynamics.

In general, as in this work, mechanical systems have triangular characteristics, which facilitates the application of this design method.

2.5.2 Backstepping Design Procedure

The Backstepping control strategy is applicable to systems which have a structure in a lower-triangular form as

$$\begin{aligned} \dot{\eta} &= f(\eta) + g(\eta)\xi \\ \dot{\xi} &= u, \end{aligned} \tag{2.54}$$

where $\eta \in \mathbf{R}$ and $\xi \in \mathbf{R}$ are the states, $f(\eta) : D \to \mathbf{R}$ and $g(\eta) : D \to \mathbf{R}$ are known nonlinear functions and $u \in \mathbf{R}$ is the control input. Therefore, before start the procedure, it is important rewritten the system to this structure. The next formulation is based on Krstic et al. [1995] and Khalil and Grizzle [2002].

Consider the second order system

$$\begin{aligned} \dot{\eta} &= f(\eta) + g(\eta)\xi \\ \dot{\xi} &= f_a(\eta,\xi) + g_a(\eta,\xi)u, \end{aligned} \tag{2.55}$$

where f_a and g_a are smooth. It is possible rewrite the system in an lower-triangular form as in (2.54) by a feedback linearization method. If $g_a(\eta,\xi) \neq 0$, the input transformation

$$u = \frac{1}{g_a(\eta,\xi)}[u_a - f_a(\eta,\xi)], \tag{2.56}$$

will reduce the system (2.55) to the follow lower-triangular form

$$\begin{aligned} \dot{\eta} &= f(\eta) + g(\eta)\xi \\ \dot{\xi} &= u_a. \end{aligned} \tag{2.57}$$

Starting from the structure (2.57), the Backstepping control procedure seeks a stabilizing virtual control law for the subsystem

$$\dot{\eta} = f(\eta) + g(\eta)\xi, \tag{2.58}$$

choosing the state ξ as a virtual control input $\phi(\eta)$, where $\phi(0) = 0$, that stabilize the dynamic of η by a CLF such that

$$\dot{V}(\eta) \leq -W(\eta) - k_1\eta^2 < 0,\ \forall \eta \neq 0,\ W(\eta) > 0,\ k_1 > 0, \tag{2.59}$$

achieving closed-loop asymptotic stability to the subsystem. In sequence, the method can be applied recursively to obtain the control input u_a in the last subsystem, such that the system will be asymptotically stability by a CLF where:

$$\dot{V}(\eta,\xi) \leq -W(\eta,\xi) - k_1\eta^2 - k_2\xi^2 < 0,\ \forall\eta \neq 0,\ \forall\xi \neq 0,\ W(\eta,\xi) > 0,\ k_1,k_2 > 0. \quad (2.60)$$

Therefore, following the theory in Krstic et al. [1995] and Khalil and Grizzle [2002], if all subsystems were globally asymptotically stable, by replacing u_a in (2.56), the original system will be globally asymptotically stable.

CHAPTER

3

METHODOLOGY

This chapter presents the methodology used to design a control system for longitudinal dynamics of vehicles, with the purpose of tracking a trajectory.

As mentioned in the previous chapter, the equation model that contains information about a given system is very important for the execution of control projects. Section 3.1 of this chapter presents the modeling for longitudinal displacement of a vehicle to obtain a set of equations for the system.

Two control methodologies will be discussed in section 3.2 for tracking a longitudinal trajectory, the Robust PID control method and the Backstepping with an integral part.

3.1 Longitudinal Dynamic Model

The longitudinal dynamic model of the vehicles is based on Newton's Laws. Analyzing the dynamic forces acting on the vehicle at Fig. 3.1, it is possible to determine the inertial force and, consequently, the acceleration along the x-axis by the summation of these forces in (3.1).

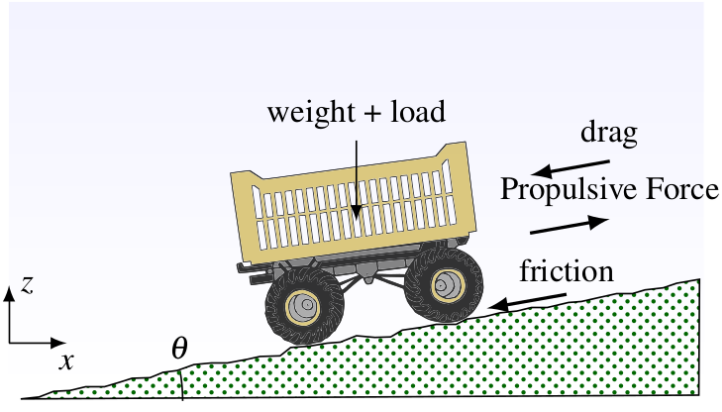

Figure 3.1 – Longitudinal forces acting on the platform navigation.

$$\vec{F}_{\text{inertial}} = \vec{F}_{\text{torque}} + \vec{F}_{\text{drag}} + \vec{F}_{\text{friction}} + \vec{F}_{\text{weight}} \tag{3.1}$$

The drag ($\vec{F}_{\text{drag}}$) and friction ($\vec{F}_{\text{friction}}$) forces absorb movement energy and, therefore, have always negative signs. The torque ($\vec{F}_{\text{torque}}$) and weight ($\vec{F}_{\text{weight}}$) forces can absorb or give energy to the movement, so their signs it will depend of the road inclination and the torque direction applied to the motor. According Rajamani [2011] and Zheng et al. [2016], the forces can be written as

$$\begin{aligned} \vec{F}_{\text{drag}} &= \frac{1}{2}\rho C_D (v - v_{wind})^2, \\ \vec{F}_{\text{friction}} &= \mu m |\vec{g}| \cos\theta, \\ \vec{F}_{\text{weight}} &= m |\vec{g}| \sin\theta, \\ \vec{F}_{\text{torque}} &= \frac{\eta}{r} T_{\text{m}}. \end{aligned} \tag{3.2}$$

We can then rewrite (3.1) as

$$ma = \frac{\eta}{r} T_{\text{m}} - \frac{1}{2}\rho C_D |v - v_{wind}|(v + v_{wind}) - \text{sgn}(v)\mu m |\vec{g}| \cos\theta - m|\vec{g}| \sin\theta, \tag{3.3}$$

where m is the mass of vehicle, ρ is the air density, C_D is the aerodynamic drag coefficient, v is the longitudinal velocity, v_{wind} is the wind velocity, $\text{sgn}(\cdot)$ is the sign function, $|\vec{g}|$ is the modulus of gravity vector, θ is the road inclination, η is the motor efficiency, r is the wheel radius, and T_{m} is the torque on tires.

The tire friction coefficient μ in (3.3) is given by Pacejka and Bakker [1992] and Pacejka [2005] as:

$$\mu = \delta \sin\left(\rho \tan^{-1}\left(\xi\kappa - \varepsilon\left[\xi\kappa - \tan^{-1}(\xi\kappa)\right]\right)\right), \tag{3.4}$$

where δ, ρ, ξ, κ and ε are coefficients given by the road and tires physical characteristics. The equation in (3.4) is called "*the magic formula*" and give us a better approximation of the friction coefficient model, as represented in Fig. 3.2, basing on the pure longitudinal slip, which include the side and longitudinal forces, and the aligning torque.

To obtain a more complete model for the longitudinal dynamics of the vehicle it is interesting to include the transmission dynamics for the electric motor of the vehicle. That model, although simplified, relates the motor torque applied with the torque at the wheels, including the energy loss due to mechanics transmissions. According to Zheng et al. [2016], it can be formally written as:

$$\zeta \dot{T}_{\text{m}} = \frac{T_u}{\beta} - T_{\text{m}}, \tag{3.5}$$

where ζ is the inertial constant, β is the transmission ratio and T_u is the motor torque.

The longitudinal model of the vehicle dynamics which will be used in future analysis takes into account some assumptions [Rajamani, 2011; Zheng et al., 2016]: i) there is no wind action, ii) the vehicle is a rigid and symmetrical body, iii) there are no yaw and roll movements, iv) there is a direct transmission from the motor to the wheels ($\beta = 1$). Besides that, the use of the

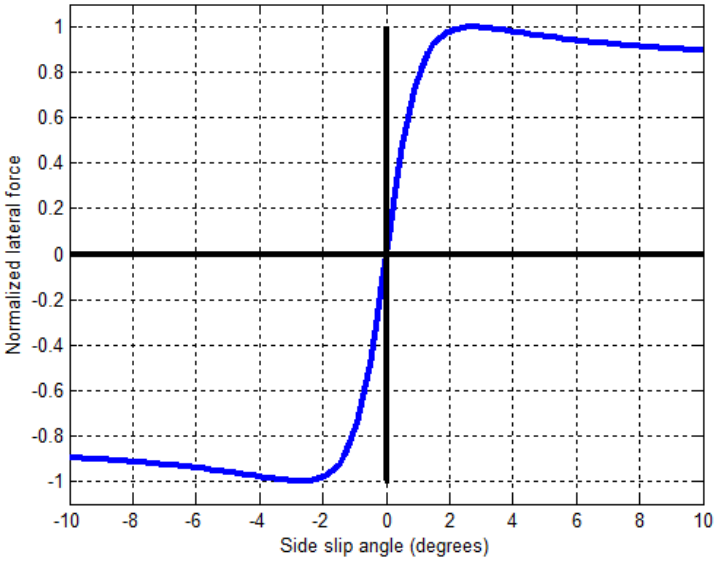

Figure 3.2 – Magic formula for $\xi = 0.714$, $\rho = 1.40$, $\delta = 1.00$ and $\varepsilon = -0.20$. Source: http://simracingpaddock.com

function $\text{sgn}(\cdot)$ in (3.3) aims to evaluate the tire friction only for $v \neq 0$, that is, when the vehicle starts its movement, bringing the model closer to reality. However, $\text{sgn}(\cdot)$ is discontinuous around zero and the use of a continuous approximation throughout the domain may avoid numerical problems. Then, $\text{sgn}(v)$ was replaced as

$$sgn(v) = \frac{(1-e^{-v})}{(1+e^{-v})} \tag{3.6}$$

Rewriting equations (3.3) and (3.5) in a state space form and including these assumptions, we have the nonlinear system:

$$\begin{cases} \dot{\vec{x}}_1 = \vec{x}_2 \\ \dot{\vec{x}}_2 = \dfrac{1}{m}\left(\dfrac{\eta}{r}\vec{x}_3 - \dfrac{1}{2}\rho C_D|\vec{x}_2|\vec{x}_2 - m|\vec{g}|\sin\theta - \dfrac{1-e^{-x_2}}{1+e^{-x_2}}m\mu|\vec{g}|\cos\theta\right), \\ \dot{\vec{x}}_3 = \dfrac{1}{\zeta}(u-\vec{x}_3) \end{cases} \tag{3.7}$$

where $\vec{x}_1$ is the longitudinal position, $\vec{x}_2$ is the longitudinal velocity, $\vec{x}_3$ is the torque and $u = T_u$ is the torque command.

Section 3.2 demonstrates the strategies to design controllers based on the model described in this section.

3.2 Trajectory Tracking Control

In Section 3.1 was presented a general longitudinal model for the vehicle studied, which will be used in the controller design. In this section will be design a longitudinal control for the vehicle, based on two strategies: a linear and a nonlinear. Both strategies aim to track a

longitudinal reference trajectory, that is, the design of the controllers will be based on the error between the position of the reference and the position of the car, trying to minimize the effect of the uncertainties and disturbances in the model.

These controller designs will be compared by software simulation and real-world experiments in a low-cost platform developed (Chapter 4), acting in adverse situations such as: a sudden change in terrain type (changes in the friction coefficient), uneven terrains (changes in slope) and addition of extra load to the vehicle (mass changes).

3.2.1 Robust PID Design

As seen in Chapter 2 the PID controller is one of the most used controllers in the industry due to its simple architecture and several tuning methods [Ge et al., 2002]. Some of these tuning methods seek to minimize the effects of uncertain parameters in the model, that is, make the controller robust to these uncertainties.

It was seen that the use of LMIs with an optimization algorithm is an effective strategy for stability analysis of high order dynamical systems with parametric uncertainties and/or disturbances. For this reason, it is a method that will be treated in this section to tune a robust PID to discontinuities and parametric uncertainties for the model described in Section 3.1.

The use of the LMIs method to PID tuning is not trivial and some alternatives can be used to facilitate. An interesting alternative is to transform the PID problem into a SOF stabilization problem and use interactive optimization algorithms to solve the LMIs subject to some project restrictions [He and Wang, 2006; Zhang et al., 2012; Zheng et al., 2016].

As known, this method applies to linear systems and it is necessary to linearize the set of equations (3.7) around an equilibrium point. An equilibrium point occurs when the system dynamics are null ($\dot{\vec{x}} = \vec{0}$) and, in this case, it will when:

$$\begin{bmatrix} \theta \\ x_2 \\ x_3 \\ u \end{bmatrix} = \begin{bmatrix} 0 \\ 0 \\ 0 \\ 0 \end{bmatrix}. \tag{3.8}$$

The $\mathscr{H}\infty$ suboptimal controller aims to minimize the effects of disturbance signals in the system (section 2.4.4). The terrain inclination it will be considered as a norm-bounded disturbance $\omega(t)$, such that the linearized system around the point (3.8) has the format:

$$\begin{cases} \dot{\vec{x}}(t) = \mathbf{A}\vec{x}(t) + \mathbf{B}_2 u(t) + \mathbf{B}_1 \omega(t) \\ \vec{z}(t) = \mathbf{C}_1 \vec{x}(t) \\ \vec{y}(t) = \mathbf{C}_2 \vec{x}(t) \end{cases}, \tag{3.9}$$

where $\vec{z}(t)$ and $\mathbf{C}_1$ are the computed output and weighting matrix, respectively, and:

$$\mathbf{A} = \begin{bmatrix} 0 & 1 & 0 \\ 0 & 0 & \frac{\eta}{mr} \\ 0 & 0 & -\frac{1}{\zeta} \end{bmatrix}, \ \mathbf{B}_2 = \begin{bmatrix} 0 \\ 0 \\ \frac{1}{\zeta} \end{bmatrix}, \ \mathbf{B}_1 = \begin{bmatrix} 0 \\ |\vec{g}|(\mu - 1) \\ 0 \end{bmatrix}, \ \mathbf{C}_2 = \begin{bmatrix} 1 & 0 & 0 \end{bmatrix},$$

$$\vec{x}(t) = \begin{bmatrix} \vec{x}_1(t) \\ \vec{x}_2(t) \\ \vec{x}_3(t) \end{bmatrix}, \text{ and } \omega(t) = \theta(t).$$

3.2.1.1 Transformation of PID to SOF control

According to Zheng et al. [2002], it is possible to transform a PID control problem into a SOF control problem by variable changes. Consider the linear time-invariant system:

$$\dot{\vec{x}} = \mathbf{A}\vec{x} + \mathbf{B}u, \quad \vec{y} = \mathbf{C}\vec{x}, \tag{3.10}$$

and the PID controller

$$u(t) = K_p\vec{y} + K_i \int_0^t \vec{y}\,dt + K_d\dot{\vec{y}}, \tag{3.11}$$

where K_p, K_i and K_d are the proportional, integral and derivative gains, respectively.

Let

$$\bar{\vec{x}}(t) = \begin{bmatrix} \vec{x}(t) \\ \int_0^t \vec{y}dt \end{bmatrix}, \qquad \dot{\bar{\vec{x}}} = \begin{bmatrix} \mathbf{A} & 0 \\ \mathbf{C}_2 & 0 \end{bmatrix} \bar{\vec{x}}, \qquad \bar{\vec{y}}(t) = \begin{bmatrix} \mathbf{C}_2\vec{x}(t) \\ \int_0^t \vec{y}dt \\ \mathbf{C}_2\mathbf{A}\vec{x}(t) \end{bmatrix} = \begin{bmatrix} \mathbf{C}_2 & 0 \\ 0 & \mathbf{I} \\ \mathbf{C}_2\mathbf{A} & 0 \end{bmatrix} \bar{\vec{x}},$$

the controller in (3.11) reduces to

$$u(t) = K_p\bar{y}_1(t) + K_i\bar{y}_2(t) + K_d\bar{y}_3(t) + K_d\mathbf{C}_2\mathbf{B}_2u, \tag{3.12}$$

and, if the Condition 1 is satisfied, a Proportional-Integral-Derivative Static Output Feedback (SOF-PID) control law can be written as [Zheng et al., 2002]:

$$\begin{aligned} u(t) &= \begin{bmatrix} (\mathbf{I} - K_d\mathbf{C}_2\mathbf{B}_2)^{-1}K_p & (\mathbf{I} - K_d\mathbf{C}_2\mathbf{B}_2)^{-1}K_i & (\mathbf{I} - K_d\mathbf{C}_2\mathbf{B}_2)^{-1}K_d \end{bmatrix} \bar{\vec{y}}(t), \\ u(t) &= \begin{bmatrix} \bar{K}_1 & \bar{K}_2 & \bar{K}_3 \end{bmatrix} \bar{\vec{y}}(t). \end{aligned} \tag{3.13}$$

Condition 1. The matrix $\mathbf{I} - K_3\mathbf{C}_2\mathbf{B}_2$ is invertible.

In the case of the model studied (3.9), the new system it will be

$$\begin{aligned} \dot{\bar{\vec{x}}}(t) &= \bar{\mathbf{A}}\bar{\vec{x}}(t) + \bar{\mathbf{B}}_2u(t) + \bar{\mathbf{B}}_1\omega(t) \\ \vec{z}(t) &= \bar{\mathbf{C}}_1\bar{\vec{x}}(t) \\ \bar{\vec{y}}(t) &= \bar{\mathbf{C}}_2\bar{\vec{x}}(t) \end{aligned} \tag{3.14}$$

where

$$\bar{\mathbf{A}} = \begin{bmatrix} \mathbf{A} & 0 \\ \mathbf{C}_2 & 0 \end{bmatrix}, \qquad \bar{\mathbf{B}}_1 = \begin{bmatrix} \mathbf{B}_1 \\ 0 \end{bmatrix}, \qquad \bar{\mathbf{B}}_2 = \begin{bmatrix} \mathbf{B}_2 \\ 0 \end{bmatrix},$$

$$\bar{\mathbf{C}}_2 = \begin{bmatrix} \mathbf{C}_2 & 0 \\ 0 & \mathbf{I} \\ \mathbf{C}_2\mathbf{A} & 0 \end{bmatrix}, \qquad \bar{\mathbf{C}}_1 = \begin{bmatrix} \mathbf{C}_1 & 0 \end{bmatrix},$$

and the control law (3.11) will be

$$u(t) = \bar{\mathbf{K}}\bar{\vec{y}}(t) \tag{3.15}$$

where

$$\bar{\mathbf{K}} = \begin{bmatrix} \bar{\mathbf{K}}_1 & \bar{\mathbf{K}}_2 & \bar{\mathbf{K}}_3 \end{bmatrix}, \tag{3.16}$$

$$K_d = \bar{\mathbf{K}}_3(\mathbf{I} + \mathbf{C}_2\mathbf{B}_2\bar{\mathbf{K}}_3)^{-1}, \tag{3.17}$$

$$K_i = (\mathbf{I} - K_d\mathbf{C}_2\mathbf{B}_2)\bar{\mathbf{K}}_2, \text{ e} \tag{3.18}$$

$$K_p = (\mathbf{I} - K_d\mathbf{C}_2\mathbf{B}_2)\bar{\mathbf{K}}_1. \tag{3.19}$$

Condition 1 is satisfied by Proposition 1, which proof is shown in Zheng et al. [2002].

Proposition 1. (Zheng, 2002). Matrix $\mathbf{I} - K_d\mathbf{C}_2\mathbf{B}_2$ is invertible if and only if $\mathbf{I} + \mathbf{C}_2\mathbf{B}_2\overline{K_3}$ is invertible, where K_d and $\overline{K_3}$ are related to each other by:

$$K_d = \overline{K_3}(\mathbf{I}_3 + \mathbf{C}_2\mathbf{B}_2\overline{K_3})^{-1}.$$

The Condition 1 and Proposition 1 is always guaranteed when $\mathbf{C}_2\mathbf{B}_2 = \mathbf{0}$, because the determinant will be different of zero ($det[\mathbf{I} - K_d\mathbf{C}_2\mathbf{B}_2] \neq 0$ and $det[\mathbf{I} + \overline{K_3}\mathbf{C}_2\mathbf{B}_2] \neq 0$). Consider the system give by (3.9), $\mathbf{C}_2\mathbf{B}_2 = \mathbf{0}$, then $\mathbf{I} + \overline{K_3}\mathbf{C}_2\mathbf{B}_2$ and $\mathbf{I} - K_d\mathbf{C}_2\mathbf{B}_2$ are not singular. Therefore, the Condition 1 and the Proposition 1 are satisfied.

In this way, it is possible to tune PID control gains from the analysis of a stability problem SOF $\mathscr{H}\infty$ by an LMI approach. However, in addition to being robust to disturbances, the goal is the controller to be robust to parametric uncertainties, so a strategy is needed to include them in the analysis.

The uncertainties of the model to be considered, as presented previously, will be: changes in the friction coefficient (μ) and mass changes (m). Analyzing the proposed linear model (3.9) and its transformation for stability analysis (3.14), the inclusion of these uncertainties results in:

$$\dot{\bar{\vec{x}}}(t) = \overline{\mathbf{A}}(\beta)\bar{\vec{x}}(t) + \overline{\mathbf{B}}_2 u(t) + \overline{\mathbf{B}}_1(\beta)\omega(t), \tag{3.20}$$

where $\beta \in \mathscr{D}$ in which β represents the uncertain parameters and $\mathscr{D}$ is a polytope of known vertices $\overline{\mathbf{A}}_i$ and $\overline{\mathbf{B}}_{1,i}$:

$$\mathscr{D} = \left\{ (\overline{\mathbf{A}}, \overline{\mathbf{B}}_1)(\beta) : (\overline{\mathbf{A}}, \overline{\mathbf{B}}_1)(\beta) = \sum_{i=1}^{k} \beta_i (\overline{\mathbf{A}}, \overline{\mathbf{B}}_1)_i ; \sum_{i=1}^{k} \beta_i = 1 ; \beta_i \geq 0 \right\},$$

$$\overline{\mathbf{A}}_i = \begin{bmatrix} \mathbf{A}_i & 0 \\ \mathbf{C}_2 & 0 \end{bmatrix}, \qquad \mathbf{A}_i = \begin{bmatrix} 0 & 1 & 0 \\ 0 & 0 & \frac{\eta}{(m+\triangle m_i)r} \\ 0 & 0 & -\frac{1}{\zeta} \end{bmatrix},$$

$$\overline{\mathbf{B}}_i = \begin{bmatrix} \mathbf{B}_{1,i} \\ 0 \end{bmatrix}, \qquad \mathbf{B}_{1,i} = \begin{bmatrix} 0 \\ |\vec{g}|(\mu + \triangle \mu_i - 1) \\ 0 \end{bmatrix},$$

where $\triangle m_i$ and $\triangle \mu_i$ are the uncertain variations of the parameters.

Transforming the model into a form to obtain the PID gains per LMI solution, we simply apply an optimization algorithm that determines these gains for model stability.

3.2.1.2 Robust PID $\mathscr{H}\infty$ Stabilization

The transformed model saw in the last section can be used to design a PID controller, robust to disturbances and uncertain parameters, solving the SOF $\mathscr{H}\infty$ stabilization problem using an LMI approach with an interactive optimization algorithm adapted from He and Wang [2006] and Zheng et al. [2002].

From last section, considering the model (3.20) in closed loop as:

$$\dot{\vec{x}}(t) = (\overline{\mathbf{A}}_i + \overline{\mathbf{B}}_2 \overline{\mathbf{K}} \overline{\mathbf{C}}_2)\vec{x}(t) + \overline{\mathbf{B}}_{1,i}\omega(t), \qquad \forall i = 1 \ldots k, \tag{3.21}$$

by the Lyapunov Stability Theory in section 2.1 and according Cao et al. [1998], Zheng et al. [2002] and He and Wang [2006]:

Lemma 1. (Cao, 1998): The system (3.21) is stabilizable via static output feedback if and only if there exist matrices $P > 0$ and $\overline{\mathbf{K}}$ satisfying the following matrix inequality:

$$\mathbf{P}(\overline{\mathbf{A}} + \overline{\mathbf{B}}_2 \overline{\mathbf{K}} \overline{\mathbf{C}}_2) + (\overline{\mathbf{A}} + \overline{\mathbf{B}}_2 \overline{\mathbf{K}} \overline{\mathbf{C}}_2)^T \mathbf{P} < 0. \tag{3.22}$$

As in Cao et al. [1998] it is possible place the eigenvalues of the system (3.21) to the left of line $\alpha/2$ in the complex plane, since exist a $P > 0$ and $\overline{\mathbf{K}}$ satisfying the following inequality:

$$\mathbf{P}(\overline{\mathbf{A}} + \overline{\mathbf{B}}_2 \overline{\mathbf{K}} \overline{\mathbf{C}}_2) + (\overline{\mathbf{A}} + \overline{\mathbf{B}}_2 \overline{\mathbf{K}} \overline{\mathbf{C}}_2)^T \mathbf{P} - \alpha \mathbf{P} < 0. \tag{3.23}$$

The $\mathscr{H}\infty$ suboptimal control, as already seen, aims to determine a control law that minimizes an upper limit for the $\mathscr{H}\infty$ norm (section 2.4.4). In case of the SOF $\mathscr{H}\infty$ stabilization

problem, it can be formally defined as finding the control law (3.15) such that the system (3.21) fulfills $\|H(s)\|_\infty < \gamma$, for $\gamma > 0$, such that, according to Cao et al. [1998], also satisfies:

$$\begin{bmatrix} \mathbf{P}\widetilde{\mathbf{A}}+\widetilde{\mathbf{A}}^T\mathbf{P}-\alpha\mathbf{P} & \mathbf{P}\widetilde{\mathbf{B}} & \widetilde{\mathbf{C}}^T \\ \widetilde{\mathbf{B}}^T\mathbf{P} & -\gamma\mathbf{I}_3 & \widetilde{\mathbf{D}}^T \\ \widetilde{\mathbf{C}} & \widetilde{\mathbf{D}} & -\gamma\mathbf{I}_3 \end{bmatrix} < 0, \tag{3.24}$$

being $\widetilde{\mathbf{A}} = (\overline{\mathbf{A}}_i + \overline{\mathbf{B}}_2\overline{\mathbf{K}}\overline{\mathbf{C}}_2)$, $\widetilde{\mathbf{B}} = \overline{\mathbf{B}}_{1,i}$, $\widetilde{\mathbf{C}} = \overline{\mathbf{C}}_1$, and $\widetilde{\mathbf{D}} = 0$. The formulation (3.24) includes (3.23), so the closed loop system will be stable if exist a matrix $\mathbf{P} = \mathbf{P}^T > 0$, an $\alpha \leq 0$ (pole allocation to the left of the complex plane) such that the constraint (3.24) is satisfied $\forall i = 1 \ldots k$ and for a minimum γ.

The constraint (3.24) is a BMI and not an LMI since there is a multiplication of the decision variables $\mathbf{P}$,α and $\overline{\mathbf{K}}$. By setting an initial matrix $\mathbf{P}$ first, it is possible to solve this constraint via an interactive LMI optimization solve the algorithm. Therefore, we have employed two algorithms, adapted from He and Wang [2006], to solve this problem. The Algorithm 1 provides an initial matrix $\mathbf{P}$, used in Algorithm 2 to calculate the SOF $\mathscr{H}\infty$ gains $\overline{\mathbf{K}}$.

Algorithm 1: Calculate $\mathbf{P}$ matrix

$i \leftarrow 1$, $\mathbf{P}_0$, $\mathbf{L}_0 \leftarrow \mathbf{I}_3$
while True **do**
  Derive $\mathbf{P}_i$ and $\mathbf{L}_i$ by solving the optimization for $\mathbf{P}_i$, $\mathbf{L}_i$, $\mathbf{V}_1 = \mathbf{P}\mathbf{B}_2\mathbf{K}$ and $\mathbf{V}_2 = \mathbf{K}\mathbf{C}_2\mathbf{L}$:
  Minimize trace($\mathbf{P}_i\mathbf{L}_{i-1} + \mathbf{L}_i\mathbf{P}_{i-1}$) subject to LMIs (3.27), (3.28) and (3.29)
  if $\left(\text{trace}(\mathbf{P}_i\mathbf{L}_i) - n\right) < \tau_1$ **then**
    $\mathbf{P} \leftarrow \mathbf{P}_i$ initial is found, **break**
  end if
  if $\left(\text{trace}(\mathbf{P}_i\mathbf{L}_i)$ - trace($\mathbf{P}_{i-1}\mathbf{L}_{i-1})\right) < \tau_2$ **then**
    $\mathbf{P}$ initial may not be found, **break**
  end if
  $i \leftarrow i + 1$
end while

In Algorithm 1 the system (3.20) was considered free of disturbances ($\omega(t) = 0$). Then, to ensure the stability of the system we need to solve the BMI problem for a $P = P^T > 0$:

$$\mathbf{P}(\overline{\mathbf{A}}_i + \overline{\mathbf{B}}_2\overline{\mathbf{K}}\overline{\mathbf{C}}_2) + (\overline{\mathbf{A}}_i + \overline{\mathbf{B}}_2\overline{\mathbf{K}}\overline{\mathbf{C}}_2)^T\mathbf{P} < 0. \tag{3.25}$$

Following He and Wang [2006], it was applied a variable change to transform it into LMIs and exclude the multiplication into $\overline{\mathbf{K}}$ and $\mathbf{P}$, such that $\mathbf{V}_1 = \mathbf{P}\overline{\mathbf{B}}_2\overline{\mathbf{K}}$, $\mathbf{V}_2 = \overline{\mathbf{K}}\overline{\mathbf{C}}_2\mathbf{L}$ and $\mathbf{L} = \mathbf{P}^{-1}$. Then

$$\begin{cases} \mathbf{P}\overline{\mathbf{A}}_i + \overline{\mathbf{A}}_i^T\mathbf{P} + \mathbf{V}_1\mathbf{C}_2 + \mathbf{C}_2^T\mathbf{V}_1^T < 0 \\ \overline{\mathbf{A}}_i\mathbf{L} + \mathbf{L}\overline{\mathbf{A}}_i^T + \mathbf{B}_2\mathbf{V}_2 + \mathbf{V}_2^T\mathbf{B}_2 < 0 \end{cases}, \tag{3.26}$$

which can be rewritten as the LMIs:

$$\begin{bmatrix} \mathbf{P}_i & \mathbf{I}_3 \\ \mathbf{I}_3 & \mathbf{L}_i \end{bmatrix} \geq 0, \tag{3.27}$$

Algorithm 2: Calculate $\overline{\mathbf{K}}$

$i \leftarrow 1$, and $\mathbf{P}_i \leftarrow \mathbf{P}$ from Alg. 1.
while True **do**
  Given $\mathbf{P}_i$, solve optimization problem for $\overline{\mathbf{K}}$
  Minimize $\alpha_i = \alpha$ subject to LMI (3.24)
  if $\alpha_i \leq 0$ **then**
    $\overline{\mathbf{K}}$ is the SOF $\mathscr{H}\infty$ stabilizing gain for γ, **break**
  else
    $i \leftarrow i+1$
    Solve optimization for $\mathbf{P}_i$ with $\overline{\mathbf{K}}$ and α_i previously found.
    Minimize trace($\mathbf{P}_i$) subject to LMI (3.24)
    if $\frac{\|\mathbf{P}_i - \mathbf{P}_{i-1}\|}{\|\mathbf{P}_i\|} < \tau_3$ **then**
      SOF $\mathscr{H}\infty$ control problem can't be solved for prescribed tolerance τ_3
    else
      $i \leftarrow i+1$ and $\mathbf{P}_i \leftarrow \mathbf{P}_{i-1}$
    end if
  end if
end while

$$\begin{bmatrix} \Gamma_{i,j} & \mathbf{P}_i\overline{\mathbf{B}}_{1,j} & \overline{\mathbf{C}}_1^T \\ \overline{\mathbf{B}}_{1,j}^T\mathbf{P}_i & -\gamma\mathbf{I}_3 & 0 \\ \overline{\mathbf{C}}_1 & 0 & -\gamma\mathbf{I}_3 \end{bmatrix}_{j=1\ldots n} < 0, \tag{3.28}$$

$$\begin{bmatrix} \Psi_{i,j} & \overline{\mathbf{B}}_{1,j} & \mathbf{L}_i\overline{\mathbf{C}}_1^T \\ \overline{\mathbf{B}}_{1,j}^T & -\gamma\mathbf{I}_3 & 0 \\ \overline{\mathbf{C}}_1\mathbf{L}_i & 0 & -\gamma\mathbf{I}_3 \end{bmatrix}_{j=1\ldots n} < 0, \tag{3.29}$$

where $\Gamma_{i,j} = \mathbf{P}_i\overline{\mathbf{A}}_j + \overline{\mathbf{A}}_j^T\mathbf{P}_i + \mathbf{V}_1\overline{\mathbf{C}}_{2,j} + \overline{\mathbf{C}}_{2,j}^T\mathbf{V}_1^T$ and $\Psi_{i,j} = \overline{\mathbf{A}}_j\mathbf{L}_i + \mathbf{L}_i\overline{\mathbf{A}}_j^T + \overline{\mathbf{B}}_2\mathbf{V}_2 + \mathbf{V}_2^T\overline{\mathbf{B}}_2^T$. Using a LMI solver, the initial value of $\mathbf{P}$ can be obtained from Algorithm 1 with stopping criteria being minimum tolerances, τ_1 and τ_2, to the trace($\mathbf{PL}$), where $\mathbf{PL} = \mathbf{I}_3$.

Algorithm 2 tries to solve the BMI problem (3.24) transforming it into an LMI by using the $\mathbf{P}$ found in Algorithm 1, thus excluding the multiplication of unknown variables. In Algorithm 2 we use the LMI solver to search for a gain matrix $\overline{\mathbf{K}}$ to the control law (3.15) for the smallest value of γ, that minimize the $\mathscr{H}\infty$ norm and consequently the disturbance effects in the system, with $\alpha < 0$, forcing the allocation of the poles in the left complex plane for stability. This is also an iterative algorithm, first using the $\mathbf{P}$ found in algorithm 1 to find a value of $\overline{\mathbf{K}}$ that minimizes α and, in case of the $\alpha > 0$, use the founded $\overline{\mathbf{K}}$ and α to find a new $\mathbf{P}$ and proceed in an iterative form until finding $\alpha < 0$.

Executing both algorithms we obtain the gain $\overline{\mathbf{K}}$ and using equations (3.19) get the PID controller gains K_p, K_i and K_d to the trajectory tracking. In Chapter 4 the results of the application of this control method into the system are treated by simulation and real-world experiments.

3.2.2 Integral Backstepping Design

This section presents a procedure design a controller via Backstepping technic with an integral action to determine a control law to the system (3.7) such that the error between the position of the robot and a virtual reference trajectory $[x_1(t) - x_r(t)]$ converges to zero in steady state.

Following the standard backstepping method as in Khalil and Grizzle [2002], it is necessary to make a variable change in the system (3.7) to format it as a superior triangular system. Let

$$u = \zeta u_n + x_3, \tag{3.30}$$

then

$$\begin{cases} \dot{\vec{x}}_1 = \vec{x}_2 \\ \dot{\vec{x}}_2 = \dfrac{1}{m}\left(\dfrac{\eta}{r}\vec{x}_3 - \dfrac{1}{2}\rho C_D|\vec{x}_2|\vec{x}_2 - m|\vec{g}|\sin\theta - \dfrac{1-e^{-x_2}}{1+e^{-x_2}}m\mu|\vec{g}|\cos\theta\right). \\ \dot{\vec{x}}_3 = u_n \end{cases} \tag{3.31}$$

Based in the procedure seen in Skjetne and Fossen [2004], Mian et al. [2008] and Rashad et al. [2015] the integral backstepping controller is formulated to solve the tracking problem $\lim_{t\to\infty}[x_1(t) - x_r(t)] = 0$ in three steps as follow.

- First Step

In the first step is chosen the backstepping states transformation as: $z_1(t) = x_r(t) - x_1(t)$ and $\xi(t) = \int_0^t z_1(\tau)d\tau$, where $z_1(t)$ is the error of position and $\xi(t)$ is the integral term of error. The dynamics afeter this transformations is:

$$\begin{aligned} \dot{\xi}(t) &= z_1(t), \\ \dot{z}_1(t) &= \dot{x}_r(t) - x_2(t). \end{aligned} \tag{3.32}$$

The following Lyapunov function is proposed to guarantee the stability of the system in (3.32)[3]:

$$V_1(\xi, z_1) = \frac{1}{2}K\xi^2 + \frac{1}{2}z_1^2, \tag{3.33}$$

where $K > 0$ and, consequently, $V_1(\xi, z_1) > 0$, $\forall\ [\xi\ z_1] \neq 0$.

To guarantee the asymptotic stability of the system, the derivative of Lyapunov function needs to be negative definite, that is, it becomes a CLF, as seen in section 2.5.1. In this way, for

$$\begin{aligned} \dot{V}_1(\xi, z_1) &= K\xi\dot{\xi} + z_1\dot{z}_1, \\ \dot{V}_1(\xi, z_1) &= z_1(K\xi + \dot{x}_r - x_2), \end{aligned} \tag{3.34}$$

[3] From this point, the time dependence (t) will be suppressed.

it is necessary to determine a state feedback virtual control law ϕ_1 such that $V_1(\xi, z_1) \leq 0$. In this step, it is chosen $\phi_1 = x_2$ and, to guarantee stability, $\phi_1 = K\xi + \dot{x}_r + C_1 z_1$ with $C_1 > 0$. Replacing in (3.34):

$$\begin{aligned} \dot{V}_1(\xi, z_1) &= z_1(K\xi + \dot{x}_r - \phi_1), \\ \dot{V}_1(\xi, z_1) &= -C_1 z_1^2 < 0, \end{aligned} \tag{3.35}$$

which is negative definite and guarantees the asymptotic stability of the system (3.32).

- Second Step

Adding and subtracting ϕ_1 in the second equation of (3.32), we have:

$$\begin{aligned} \dot{\xi} &= z_1, \\ \dot{z}_1 &= \dot{x}_r - \phi_1 + (\phi_1 - x_2) = -K\xi - C_1 z_1 + (\phi_1 - x_2). \end{aligned} \tag{3.36}$$

Making a change of variables $z_2 = x_2 - \phi_1$, a new system can be rewritten as:

$$\begin{aligned} \dot{\xi} &= z_1, \\ \dot{z}_1 &= \dot{x}_r - \phi_1 + (\phi_1 - x_2) = -K\xi - C_1 z_1 - z_2, \\ \dot{z}_2 &= \left(\frac{\eta}{mr} x_3 - \frac{1}{2}\rho C_D |x_2| x_2 - |\vec{g}| \sin\theta - \frac{1 - e^{-x_2}}{1 + e^{-x_2}} \mu |\vec{g}| \cos\theta \right) - \dot{\phi}_1, \end{aligned} \tag{3.37}$$

where

$$\dot{\phi}_1 = K z_1 + \ddot{x}_r - C_1(z_2 + K\xi + C_1 z_1). \tag{3.38}$$

Consider a new Lyapunov function as

$$V_2(\xi, z_1, z_2) = V_1(\xi, z_1) + \frac{1}{2} z_2^2 > 0, \ \forall \ [\xi \ z_1 \ z_2] \neq 0, \tag{3.39}$$

which has the following derivative:

$$\begin{aligned} \dot{V}_2(\xi, z_1, z_2) &= K\xi\dot{\xi} + z_1\dot{z}_1 + z_2\dot{z}_2, \\ \dot{V}_2(\xi, z_1, z_2) &= -z_1 z_2 - C_1 z_1^2 + z_2 \left(\frac{\eta}{mr} x_3 - \frac{1}{2}\rho C_D |x_2| x_2 - |\vec{g}| \sin\theta \right. \\ &\quad \left. - \frac{1 - e^{-x_2}}{1 + e^{-x_2}} \mu |\vec{g}| \cos\theta - \dot{\phi}_1 \right). \end{aligned} \tag{3.40}$$

Then, to guarantees the asymptotic stability it is necessary a virtual control law ϕ_2, in this case will be x_3, which makes $\dot{V}_2(\xi, z_1, z_2) < 0$. Therefore,

$$\phi_2 = \frac{mr}{\eta} \left(\frac{1}{2}\rho C_D |x_2| x_2 + |\vec{g}| \sin\theta + \frac{1 - e^{-x_2}}{1 + e^{-x_2}} \mu |\vec{g}| \cos\theta + \dot{\phi}_1 + z_1 - C_2 z_2 \right) \tag{3.41}$$

and replacing in (3.40) we have $\dot{V}_2 < 0 \ \forall \ [z_1 \ z_2]$ since that $C_1 > 0$ and $C_2 > 0$:

$$\dot{V}_2(\xi, z_1, z_2) = -C_1 z_1^2 - C_2 z_2^2 < 0. \tag{3.42}$$

- Third Step

Following the same approach used in the last step, a variable change is made as $z_3 = x_3 - \phi_2$ and a new system can be rewritten as:

$$\begin{aligned} \dot{\xi} &= z_1, \\ \dot{z}_1 &= -z_2 - K\xi - C_1 z_1, \\ \dot{z}_2 &= \frac{\eta}{mr} z_3 + z_1 - C_2 z_2, \\ \dot{z}_3 &= u_n - \dot{\phi}_2, \end{aligned} \tag{3.43}$$

where

$$\begin{aligned} \dot{\phi}_2 = \frac{mr}{\eta} \Bigg[& \rho C_D |x_2| x_2 + |\vec{g}| \sin\theta + \mu |\vec{g}| \cos\theta \frac{2e^{-x_2}}{(1+e^{-x_2})^2} \dot{x}_2 + \dot{z}_1 (K+1) \\ & + \dddot{x}_r - C_1 (\dot{z}_2 + K\xi + C_1 z_1) - C_2 \dot{z}_2 \Bigg]. \end{aligned} \tag{3.44}$$

A new Lyapunov function it is necessary to evaluate the system stability. Thus,

$$V_3(\xi, z_1, z_2, z_3) = V_2(\xi, z_1, z_2) + \frac{1}{2} z_3^2, \tag{3.45}$$

where $V_3(\xi, z_1, z_2, z_3) > 0 \; \forall \; [\xi \; z_1 \; z_2 \; z_3] \neq 0$.

To be asymptotically stable, the derivative of the Lyapunov function needs to be negative definite. In this way, it is necessary a control law that guarantees $\dot{V}_3 < 0$. Being

$$\dot{V}_3(\xi, z_1, z_2, z_3) = -C_1 z_1^2 - C_2 z_2^2 + \frac{\eta}{mr} z_2 z_3 + z_3 (u_n - \dot{\phi}_2), \tag{3.46}$$

let choose

$$u_n = \dot{\phi}_2 - \frac{\eta}{mr} z_2 - C_3 z_3 \tag{3.47}$$

such that, by replacing (3.47) in (3.46),

$$\dot{V}_3(\xi, z_1, z_2, z_3) = -C_1 z_1^2 - C_2 z_2^2 - C_3 z_3^2. \tag{3.48}$$

Therefore, by inspection $\dot{V}_3 < 0 \; \forall \; [z_1, \; z_2, \; z_3] \neq 0$, since $[C_1 C_2 C_3] > 0$. Then, according the Lemma presents in Khalil and Grizzle [2002], Krstic et al. [1995] and as show in Skjetne and Fossen [2004], Mian et al. [2008] and Rashad et al. [2015], replacing (3.47) into (3.30), the system (3.7) will be globally asymptotically stable for a bounded reference input x_r and guarantees that $\lim_{t\to\infty}[x_1(t) - x_r(t)] = 0$.

In Chapter 4, simulated and real-world experiments will be presented to evaluate the proposed method.

3.3 Platform Design

To realize experiments in a real-world scenarios, it was built a small robot over the *Mad Force Kruiser 2.0 1/8 Monster Truck* platform show in Fig. 3.3. The platform was built with a *Raspberry Pi 3* computer with *Ubuntu Mate 18.04* to process data and compute control actions executing a framework designed into Robot Operating System (ROS)[4] Kinetic, presented in Fig. 3.4, with algorithms implemented in *Python* and *C++* languages.

Figure 3.3 – Mad Force Kruiser 2.0 1/8 Monster Truck. Source: rc.kyosho.com

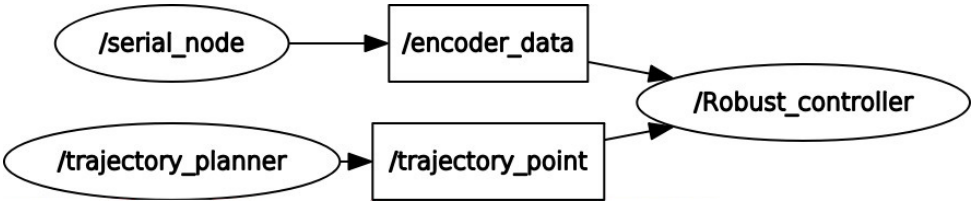

Figure 3.4 – Control architecture at the ROS.

The feedback information is provided by a digital incremental rotary encoder *LPD3806-360BM*, coupled in an intermediate reduction between the motor's shaft and the wheel. The used encoder has a high resolution (360 pulses per revolution), therefore, it was necessary to put it into a reduction of the motor to reduce the reading frequency and do not overload the system. Moreover, for the same reason, an *Arduino Nano* micro-controller it is used, exclusively, to read the encoder information, calculating the robot odometry and send it via serial communication to the *Raspberry*, reducing the work done with this last. A sampling frequency of $20Hz$ is provided by Arduino for encoder measurements. However, this frequency is limited to $10.0Hz$ by the control node because of the delay required to change the motor rotation direction (foward and reverse).

The torque command is ensured by an Electronic Speed Controller (ESC), operated via Pulse Width Modulation (PWM) inputs come from the embedded computer and pass through

[4] www.ros.org/kinetic/

an *Adafruit PCA9685* motor driver, with 12 bits (0 - 4095) of resolution and 50 Hz, before it reaches the ESC. As the control input used in the model is the torque applied to the motor ($N.m$) and the control input of the robot, which influences the motor rotation, is PWM, it was necessary a previous calibration to relate the two quantities.

The calibration was done using the least squares method to estimate a linear function that relates the torque in the motor and the PWM value (bits) sent to the ESC. First, a data set was generated by applying a sequence of bits (PWM) to the ESC and collecting the force (N) applied to the wheel axis from a digital force sensor, which has been positioned in a lever with distance $L = 0.14\ m$ from the wheel axis. Thus, by using the equation ($Torque = Force\ x\ distance$), it was possible to collect five samples with 10 observations each in two sets, one computed in the forward direction and another in the reverse. The number of observations was established by the limitation of the measuring apparatus, the Tables 3.1 and 3.2 show these data sets considering the calculation of the torque from the force measured and the lever distance L.

Considering a transmission ratio 7.8 : 1 from the motor axis to the wheel axis and using the least squares method, the linear functions that relate PWM and Torque can be express as

$$\begin{aligned} PWM_{forward} &= 379.02 + 4.21(T_{forward}), \\ PWM_{reverse} &= 353.69 - 10.86(T_{reverse}). \end{aligned} \tag{3.49}$$

where T is the motor torque, PWM is the value sent to the ESC and the terms “forward” and “reverse” reflect the direction of rotation.

Table 3.1 – Data set for calibration in the forward direction.

PWM	Sample-1(N.m)	Sample-2(N.m)	Sample-3(N.m)	Sample-4(N.m)	Sample-5(N.m)
384	1.372	1.509	1.509	1.784	1.509
386	2.332	2.058	2.195	1.784	2.058
388	2.470	2.195	2.195	2.607	2.195
390	2.607	2.744	2.744	3.018	2.881
392	3.704	3.430	3.704	3.430	3.293
394	3.842	3.979	4.253	3.979	3.567
396	3.979	3.842	4.390	4.253	4.253
398	4.390	3.979	4.253	4.390	4.116
400	4.665	4.665	4.528	4.665	4.665
402	4.528	4.939	4.802	4.939	4.802

Table 3.2 – Data set for calibration in the reverse direction.

PWM	Sample-1(N.m)	Sample-2(N.m)	Sample-3(N.m)	Sample-4(N.m)	Sample-5(N.m)
344	0.823	0.823	0.823	0.823	0.823
342	0.823	0.960	0.960	0.960	0.823
340	1.372	1.098	1.235	1.098	0.960
338	1.509	1.372	1.372	1.372	1.235
336	1.784	1.646	1.784	1.646	1.646
334	2.058	1.921	2.058	1.921	1.921
332	1.921	2.058	1.921	2.058	1.921
330	2.058	2.058	1.921	2.058	2.058
328	2.195	2.058	2.058	2.058	2.195
326	2.195	2.195	2.332	2.195	2.332

The control of the robot is made using all of these devices boarded and a battery pack to powering these (ESC-Motor power was provided by a secondary battery). Besides that, some pieces were created in a 3D printer (Prusa I3) to connect these devices into the robot. Fig. 3.5 show a flowchart of the control operation with the employed devices.

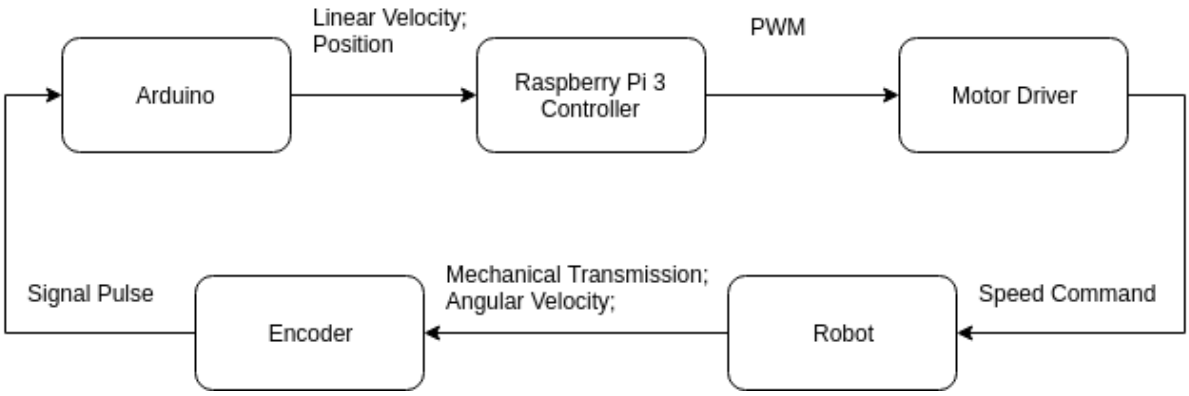

Figure 3.5 – Flowchart of the control operation.

CHAPTER

4

RESULTS

This chapter presents simulated and real-world results of the controllers presented in last sections, applied to a longitudinal trajectory tracking problem with irregular terrains. The goal is evaluate and compare both methods applying them to the model present in section 3.1 by a simulation using the software *MATLAB*® and to a low-cost platform developed for experiments. In both experiments were used the characteristics of the *Mad Force Kruiser 2.0 1/8 Monster Truck* (vide Fig. 1.5 and Section 3.3), the table 4.1 describes all the parameters used.

Table 4.1 – Model parameters used in the simulator.

Parameter	**Value**	**Unity**	**Parameter**	**Value**	**Unity**
Mass (m)	5.50	Kg	Gravity ($\|\vec{g}\|$)	9.81	m/s^2
Air density (ρ)	1.18	Kg/m^3	Drag coeff. (C_D)	0.10	[ ]
Wheel radius (r)	0.08	m	Motor efficiency (η)	95.00	%
Road angle (θ)	0.00	rad	Torque inertia (ζ)	0.10	[ ]

To evaluate the robustness of the controllers, it has also compiled some extreme values of tire friction, concerning Eq. (3.4) and illustrated in Table 4.2, to compose the polytope of the robust estimation. These friction values were based on data of the literature[5] and the mass of the robot measured with a weight balance.

Table 4.2 – Range of parameters uncertainties: vertices of the polytope.

Ground-type	μ	**Vehicle's mass**	m[kg]
dry tarmac	0.36	unloaded	5.50
uneven ground with tall grass	1.54	loaded	8.00

The purpose of the experiments is to evaluate the behavior of the robot following a virtual reference trajectory with controllers action. The chosen reference trajectories will be planned

[5] https://www.mathworks.com/help/physmod/sdl/ref/tireroadinteractionmagicformula.html

as third-order polynomial functions and this planning method it will be shown in the following section.

4.1 Reference Trajectory Planning

The set-point trajectory for the robot is based only on longitudinal movements. The basic objective of this generation is to move the robot from an initial position to a final position. In general, we can represent a trajectory as a polynomial time function which the order depends on the number of constraints inserted in the planning. For the experiments that were performed, third-order polynomial functions were used, considering the initial position, the goal position and the time duration of the trajectory.

These polynomial trajectories are formed by an initial position x_0, a final position x_f and the time t_f spent to travel from x_0 to x_f. In this way we will have four obvious constraints come from x_0, x_f and another two to the velocity at the start point and at the end:

$$\begin{aligned} x(0) &= x_0, \quad x(t_f) = x_f, \\ \dot{x}(0) &= 0, \quad \dot{x}(t_f) = 0. \end{aligned} \tag{4.1}$$

Following the method in Craig [2004], these four constraints can be satisfied by a third order polynomial function as

$$\begin{cases} x(t) = a_0 + a_1 t + a_2 t^2 + a_3 t^3 \\ \dot{x}(t) = a_1 + 2a_2 t + 3a_3 t^2 \end{cases}, \tag{4.2}$$

where $a_0 = x_0$, $a_1 = 0$, $a_2 = \frac{3}{t_f^2}(x_f - x_0)$ and $a_3 = -\frac{2}{t_f^3}(x_f - x_0)$. The main advantage of using smooth trajectories at this application is the avoiding of abrupt jerks in the vehicle's engine.

A higher-order polynomial can be used if it were of interest to add constraints for initial and final acceleration, for example. But for the experiments performed here the one presented in (4.2) was sufficient.

4.2 Simulated Results

Firstly, the controllers gains were calculated using the methods seen in Chapter 3. In the robust PID case, the algorithms developed in Section 3.2.1 were solved by using the *MOSEK* solver[6] in software *MATLAB*® and the uncertainties used as vertices of the polytope (3.20) were those described in Table 4.2. In the *Backstepping* case, using the method in Section 3.2.2, the control gains were chosen, respecting the presented stability constraints. The controllers gains obtained are show in Table 4.3.

[6] The MOSEK optimization software: `https://www.mosek.com/`.

Table 4.3 – Controllers gains.

Controller	**Gains**			
Robust PID	K_p	K_i	K_d	
	14.20	13.90	5.01	
Backstepping	K	C_1	C_2	C_3
	1.00	1.00	7.00	8.00

The simulations were made using a simulator implemented in *Simulink/MatLab* tool, where the system dynamics (3.7) has been tested in a closed loop by applying the control law of the developed controllers. Some scenarios have been tested to analyze the control systems in an ideal condition and with disturbances. In the scenario called as an ideal, it is consider that the system operates in a dry tarmac with a friction coefficient as in Table 4.2, without changes in the parameters of Table 4.1, no disturbances in the inclination of the road ($\theta = 0$) and with small measurement noises. It was applied a polynomial trajectory to move the robot 40 m forward and backward in 30 seconds each. Fig. 4.1 shows the comparative results of both controllers for position and speed of the simulated vehicle in the ideal scenario.

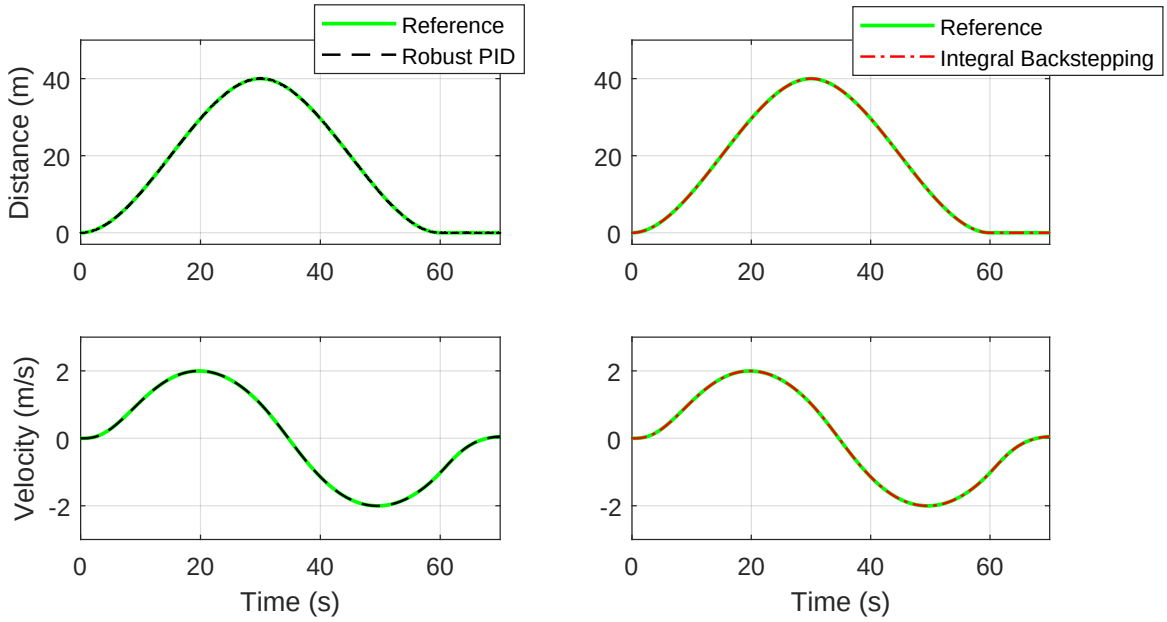

Figure 4.1 – Simulation results without uncertainties.

It is possible to see that both controllers correspond to the objective of tracking the trajectory and reject the noise at the measured output. Analyzing the distance error between the reference and the position output at Fig. 4.2, it is possible to note that the integral Backstepping presents an error mean smaller than the robust PID, but both approaches zero.

To analyze the robustness of the controllers, other scenarios have been tested, applying changes in the terrain conditions, varying the mass of the vehicle in a typical load transporta-

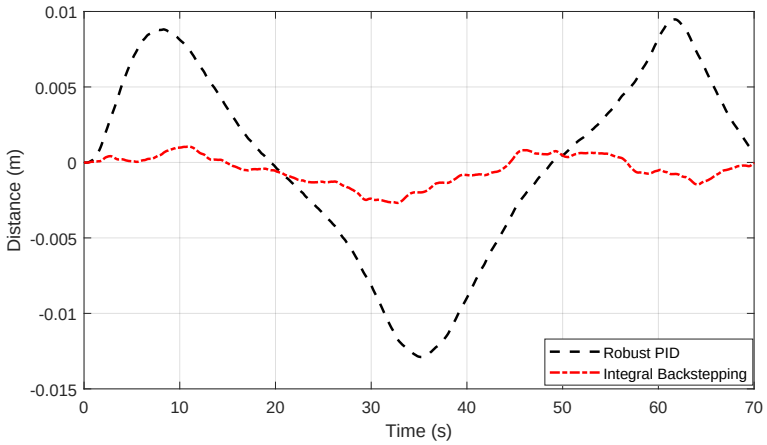

Figure 4.2 – Simulation position error results without uncertainties.

tion mission and keeping the measurement noises. In the second simulation, the scenario of uncertainties described in Table 4.4 was used.

Table 4.4 – Scenarios of simulation 2: mass m variation, slope θ, and friction μ.

Scenario	m [kg]	$\theta[^\circ]$	μ
S0	5.5	0	0.848
S1	5.5	28	1.543
S2	6.5	28	1.543
S3	7.5	-28	1.543
S4	7.5	0	0.848

Fig. 4.3 shows the results for position and speed of the simulated vehicle, respectively, while Fig. 4.4 illustrates the tracking error and the torque applied by the controllers. It can be seen that the robust PID controller minimizes the disturbances (ground slopes) and the parametric uncertainties (mass variation and friction) better than the *Backstepping* controller. Although both ensure null error in steady state, the robust PID converges faster and, analyzing Fig. 4.4, it is noticed that the error between the reference and the measured displacement is almost null during all trajectory, using the PID controller. Calculating the mean square error (MSE) in both cases, we have 0.490 using the *Backstepping* controller and 0.067 for the PID, proving the previous analysis.

Another simulation has been done using a different trajectory, now representing a bumpy terrain. In this simulation, the terrain inclination was arbitrarily changed along the trajectory within the interval $[-30^\circ, 30^\circ]$ (negative and positive slopes), and the friction was varied within the range shown in Table 4.2. Also, the mass was changed by adding 1 kg to the bodywork at in each stop of the trajectory (exceeding the limit of 8 kg used in the Robust PID controller design). Figures 4.5 and 4.6 show the results of this third simulation. Once more, the trajectory was satisfactorily tracked by both controllers, despite terrain conditions, and the error using the robust PID controller was lower, as evidenced by the calculation of the MSE where it was

obtained 0.244 for the *Backstepping* and 0.065 for the PID.

The difference in the controller's performance was evaluated using the Integral Absolute Error (IAE), Integral Time Absolute Error (ITAE), Integral Square Error (ISE) and Integral Time Square Error (ITSE) indexes. The Table 4.5 shows a mean of these indexes for each controller in the simulations(excluding the ideal scenario), calculated by the equations:

$$IAE = \int_0^T |e(t)|\, dt; \quad ITAE = \int_0^T t|e(t)|\, dt;$$
$$ISE = \int_0^T e(t)^2\, dt; \quad ITSE = \int_0^T te(t)^2\, dt.$$

These indexes evaluate the performance of the controllers in converging to a proposed reference and the time spent in this convergence. Observing the indexes, it is possible to notice that the Robust PID has the lowest values for them, what translate the better results of performance.

Table 4.5 – Average performance indices from the experiments for each controller.

Controller	IAE	ITAE	ISE	ITSE
Integral Backstepping	19.89	831.38	22.61	22.77
Robust PID	3.34	140.64	0.75	0.75

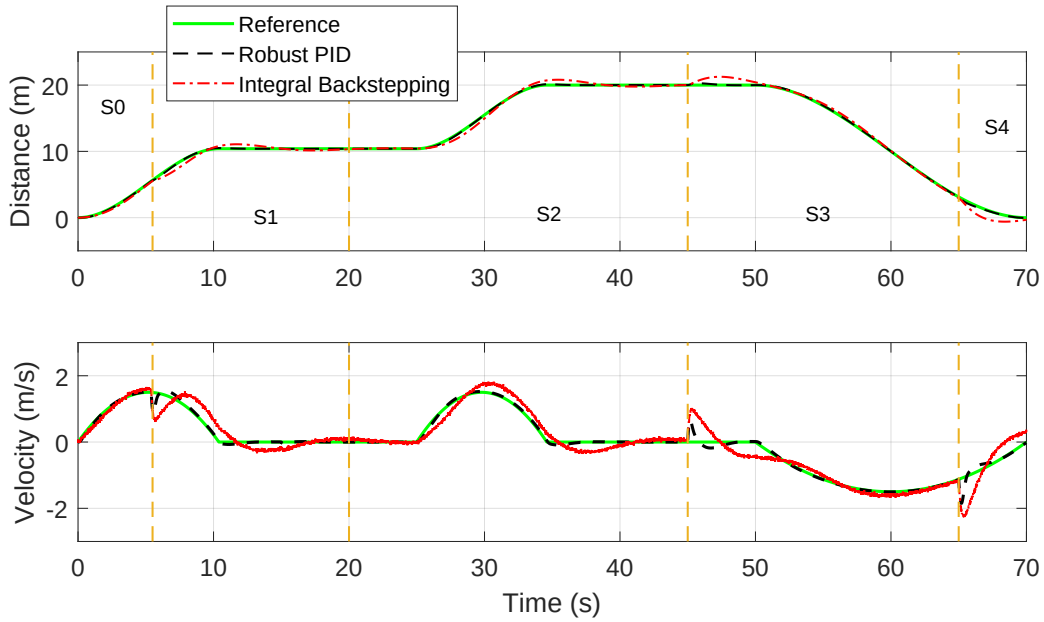

Figure 4.3 – Simulation results of Table 4.4: position and speed trajectory.

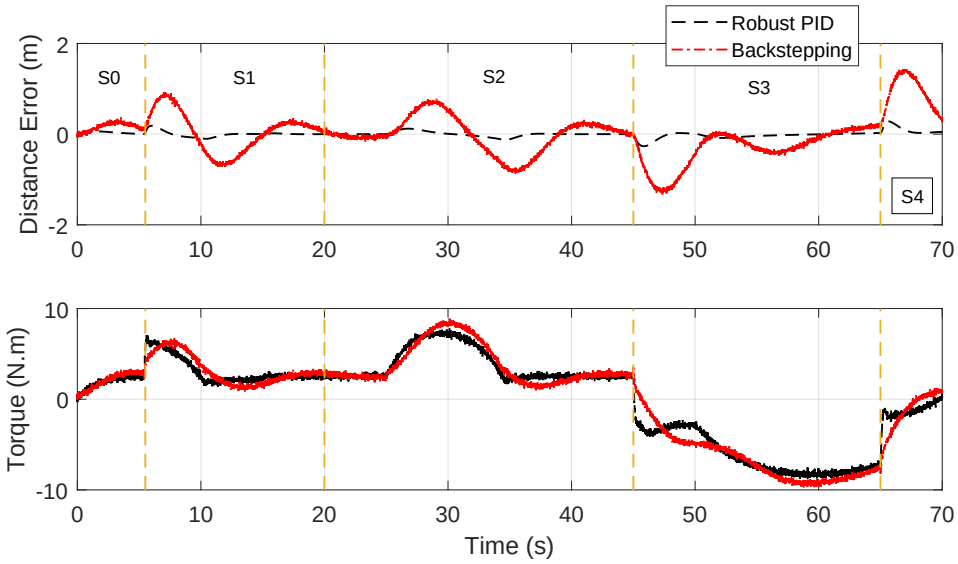

Figure 4.4 – Simulation results of Table 4.4: position error and torque.

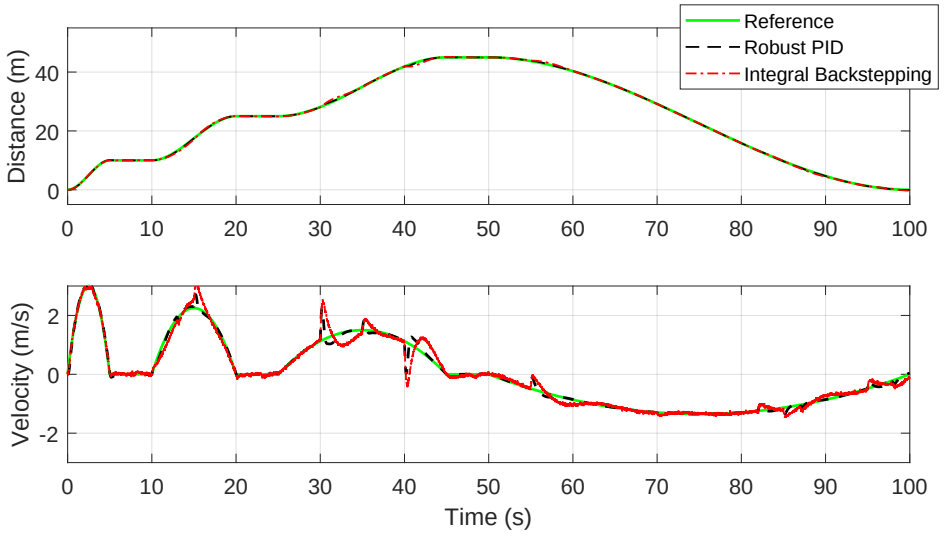

Figure 4.5 – Simulation results of Table 4.4: position and speed trajectory.

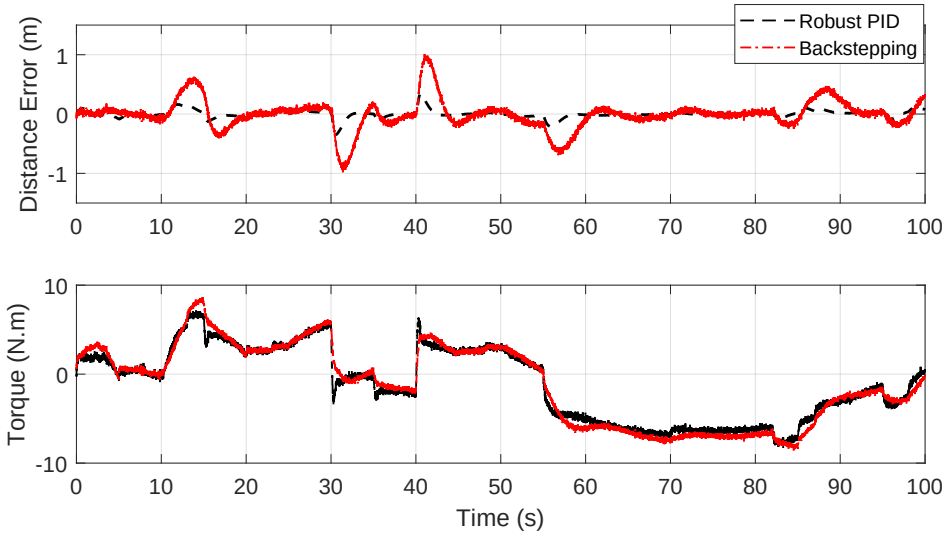

Figure 4.6 – Simulation results of Table 4.4: position error and torque.

4.2.1 Backstepping Method Issues

The values of the Backstepping controller gains are not well defined by the method. The choice of them (Table 4.3) was made based on experiments, respecting the criteria of the method that, in this case, requires positive gains for asymptotic stability. The Fig. 4.7(a) and 4.7(b) show experiments in the ideal scenario for some values of gains. The performance of the controller was not as expected. The Fig. 4.8 shows another simulation using other gains and obtaining better results tracking the reference, but with problems in the control signal and speed tracking. It is possible to note that the controller is sensitive to the choice of the gains, despite respect the stability criteria. This problem does not occur with the PID controller, since the gains are well defined by the design.

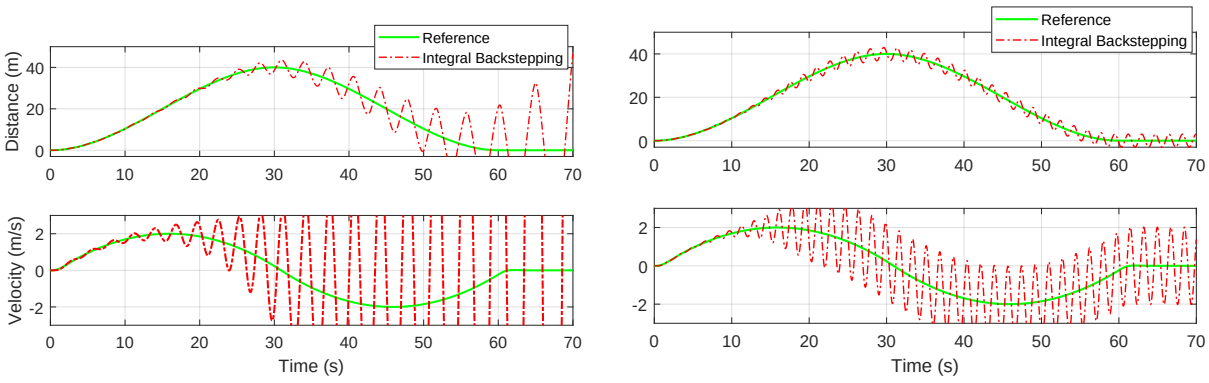

(a) (b)

Figure 4.7 – Integral Backstepping simulation in an ideal scenario with gains: (a) $[K, C_1, C_2, C_3] = [10, 5, 1, 1]$ and (b) $[K, C_1, C_2, C_3] = [5, 10, 5, 1]$

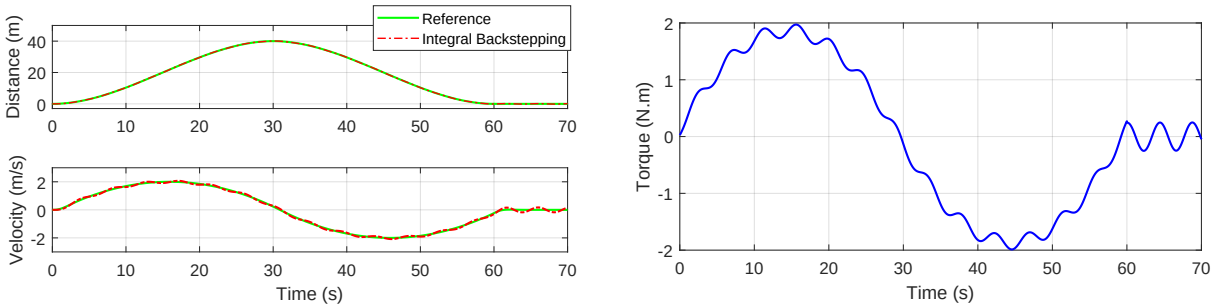

(a) (b)

Figure 4.8 – Integral Backstepping simulation in an ideal scenario with $[K, C_1, C_2, C_3] = [2, 1, 1, 2]$, where (a) is the Distance and velocity response and (b) the control signal.

4.3 Real World Results

This section presents real-world results of the controllers of the chapter 3, applied to the control system of the platform developed show in section 3.3. The results of the Robust PID and the Integral Backstepping were compared with each other to evaluate the performance in the execution of objective.

The purpose of the experiments is to reflect a typical mission of payload delivery in uneven terrains. Thus, the robot must track a smooth longitudinal trajectory that promotes a displacement in both directions (forward and backward), executed in terrains with different configurations, ranging from soft-ground to tall grass in uneven soil, illustrated in Figures 4.9(a) to 4.9(d), and with extra loads, represented by two dumbbells of 1 kg, added to the vehicle during some stops. In these experiments, we seek to evaluate the effect of these adverse conditions on the system and the performance of each controller. In this case, the torque (state x_3 in the model (3.7)) is not measured and it is considered that the PWM value send to ESC is equivalent to the torque applied, obtained from calibration (3.49).

The realization of these experiments require a digital control system acting in the Raspberry PI 3 used in the platform development (section 3.3). Therefore, it is used a bilinear transform method to obtain a discrete-time representation from the continuous-time representation of developed Robust PID controller. This was possible due to the high sample rate in reading position and velocity data, as presented in section 3.3. Table 4.6 shows gains obtained after discretization using a frequency of $10.0Hz$.

Table 4.6 – Discrete Controllers gains.

Controller	**Gains**		
Robust PID	K_p	K_i	K_d
	14.90	13.90	5.01

(a) dirt road floor

(b) grass

(c) soft-ground

(d) bumpy terrain

Figure 4.9 – Experiments with the prototype in different fields.

Firstly, two missions have been tested, which are described in Table 4.7. All controllers are tested in the same mission and the results are shown in Figures 4.10 and 4.11, which represents the trajectory traveled and the speed employed in the mission 1 and 2, respectively.

Table 4.7 – Scenarios of missions: mass variation, slope profile and terrain type.

Scenario	m [kg] (mission)		slope $\approx 20^\circ$	ground-type
	1	2		
S1	5.5	7.5	no slope	plane stones
S2	5.5	7.5	climbing	tall grass
S3	6.5	6.5	climbing	tall grass
S4	7.5	5.5	descending	tall grass
S5	7.5	5.5	no slope	plane stones

Another experiment was performed in a bumpy dirt road, submitting the robot to a path with holes and small obstacles like: sticks, stones, and leaves. The same trajectory was passed as a reference to the controllers and the mission scenarios are described in Table 4.8. The exactly

ground inclination present in these experiments is unknown, but it is known that is smaller (almost zero) than the missions in Table 4.7. The results are shown in Figures 4.12 and 4.13.

Table 4.8 – Scenario description of the experiments on the bumpy road.

	m [kg]	
Scenario	(mission 1)	(mission 2)
S1	5.5	7.5
S2	6.5	6.5
S3	7.5	5.5

Analyzing the results, it is possible to notice that the robot follows the trajectory with both controllers. In adverse situations, present in all missions of the experiment, it is possible to notice that the Integral Backstepping controller have more difficulties to reject the disturbances (ground slopes) and the uncertainties of the parameters (change of mass and soil type) than the robust PID. It is clear that the PID was designed to be robust to these adversities, but the Integral Backstepping takes on the nonlinearities of the system, different of the PID that uses the linearized model. Therefore, even using a more complete model, the Integral Backstepping controller demonstrates a worse performance.

This difference between the controllers is shown in Fig. 4.14, which shows the distance error between the reference and the measurement of each controller. Note that the average of the PID controller error is lower in all experiments.

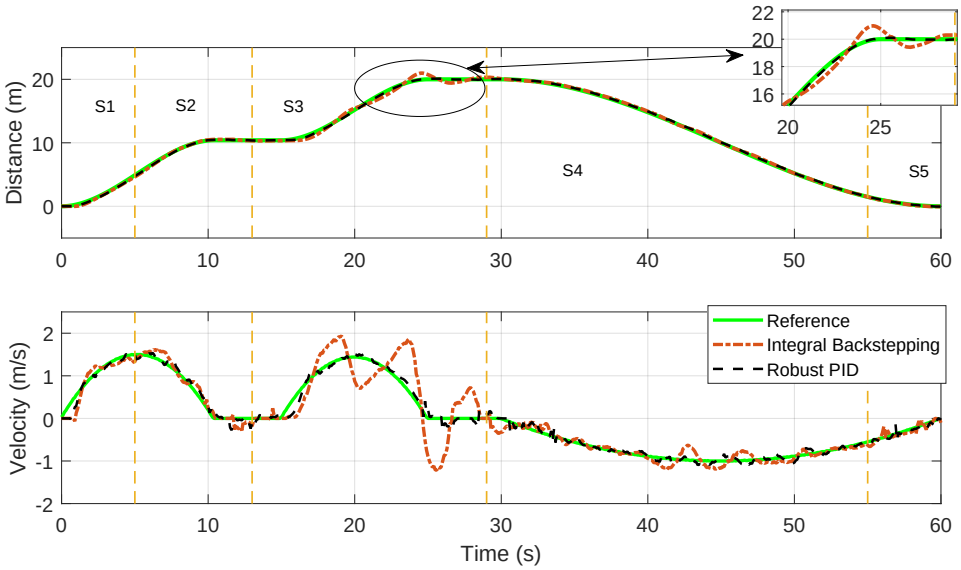

Figure 4.10 – Results of mission 1 (Table 4.7): position and speed of Reference and all tested controllers.

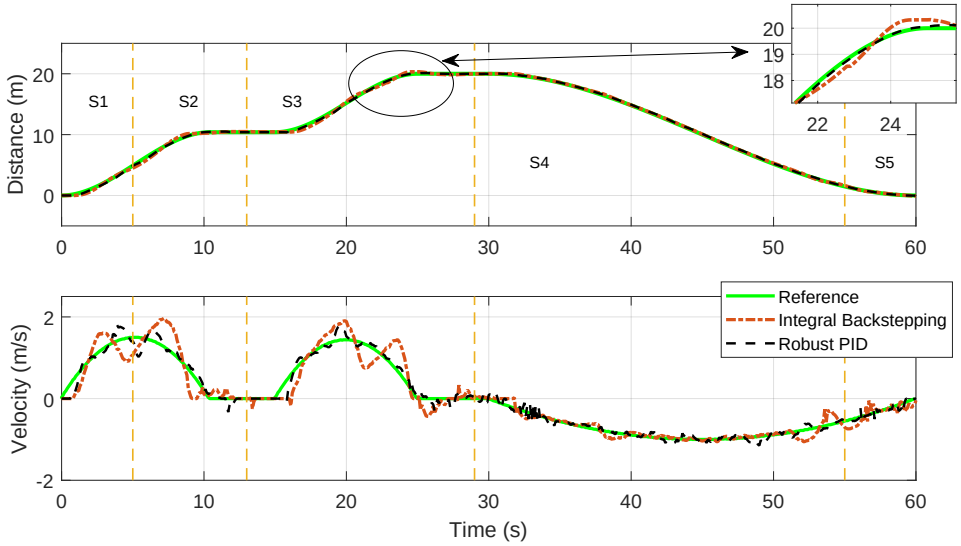

Figure 4.11 – Results of mission 2 (Table 4.7): position and speed of Reference and all tested controllers.

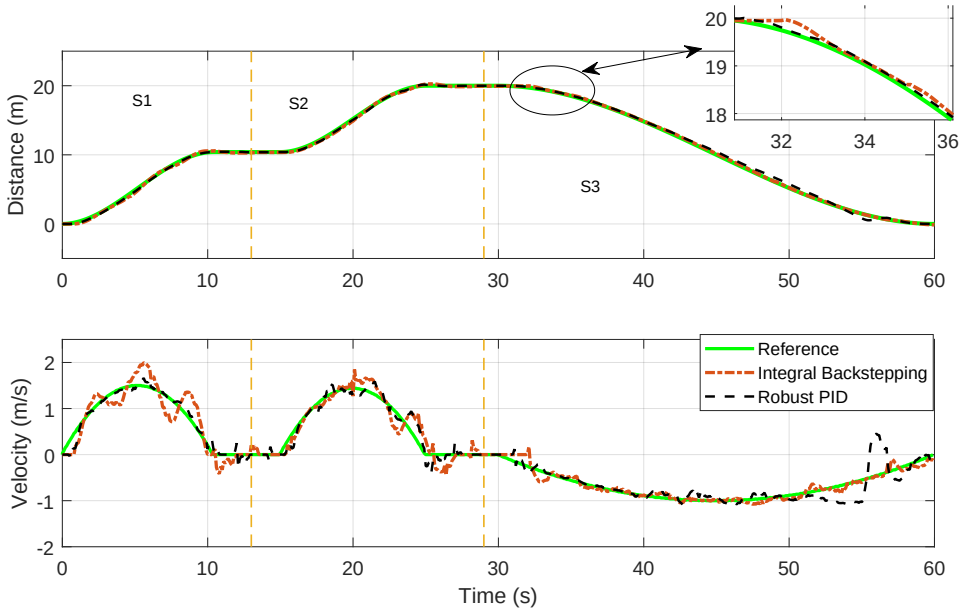

Figure 4.12 – Results of mission 1 (Table 4.8): position and speed of Reference and all tested controllers.

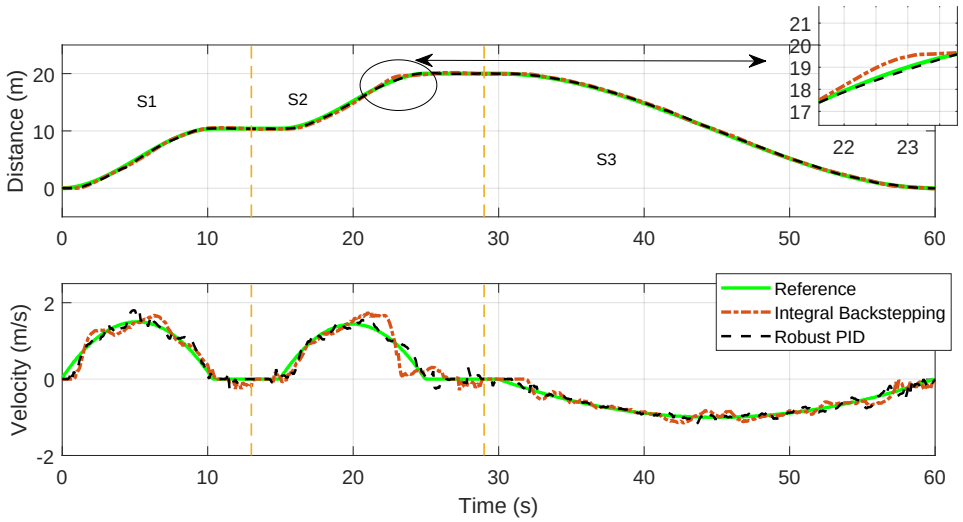

Figure 4.13 – Results of mission 2 (Table 4.8): position and speed of Reference and all tested controllers.

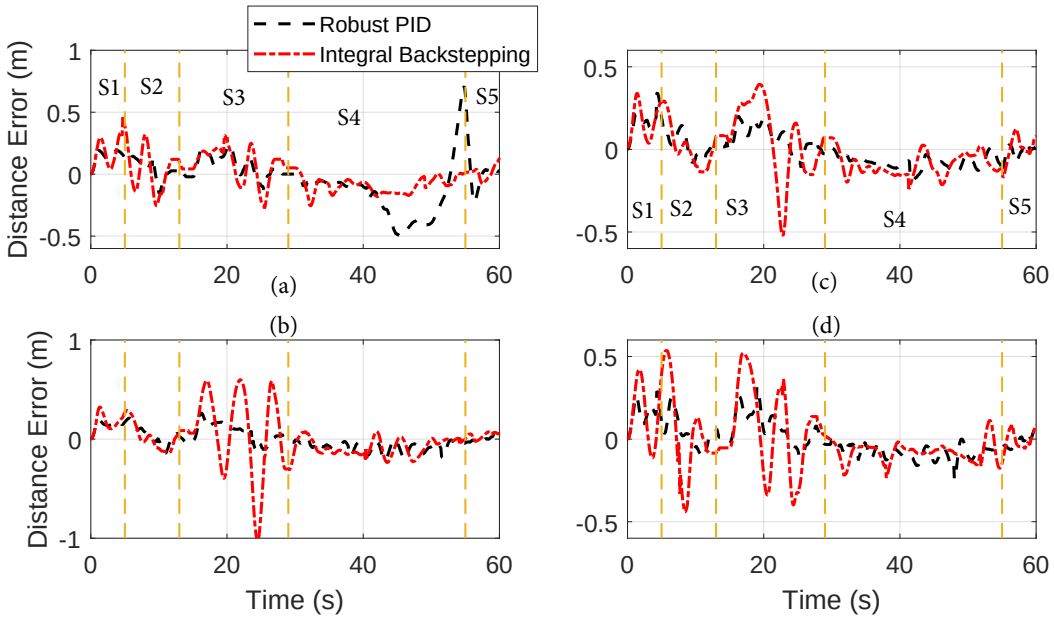

Figure 4.14 – Results of distance error in (a) mission 1 (Table 4.7); (b) mission 2 (Table 4.7); (c) mission 1 (Table 4.8); and (d)mission 2 (Table 4.8)

The difference of the controller's performance was evaluated using the IAE, ITAE, ISE and ITSE indexes. The Table 4.9 shows a mean of these indexes for each controller in all missions of the experiments. Observing the indexes, it is possible to notice that the Robust PID has the lowest values for them, what translate the better results of performance.

Table 4.9 – Average performance indices from the experiments for each controller.

Controller	IAE	ITAE	ISE	ITSE
Integral Backstepping	8.13	198.42	4.19	4.28
Robust PID	5.79	174.83	2.12	2.14

CHAPTER

5

CONCLUSION

This work approached the problem of longitudinal trajectory tracking by a ground robot semi autonomously in uneven terrains, typical of some applications in agricultural environments, mining, exploration, among others. The solution involved the development of two controllers by different methodologies: a Robust PID and an Integral Backstepping, which were compared in simulated experiments and in real-world missions of payload delivery on longitudinal trajectories. The realization of the real experiments involved the development of a four-wheeled platform with an embedded system capable of executing the controllers developed in adverse situations as that cited.

The experiments were designed to evaluate the performance of both controllers in the presence of parametric uncertainties (mass and friction changes) and external disturbances (terrain slopes). The results showed that both controllers are able to reduce the tracking error. Therefore, even using a simplified linear model, the robust PID rejected better the disturbances and the uncertainties with a simpler tuning method, especially when analyzing the behavior of the speed employed during the experiments and the distance error. Performance indices also demonstrate the superiority of the robust PID controller. We should emphasize that the Integral Backstepping, in ideal conditions (parameter values do not change), obtained a better result in the simulation.

Besides that, it can be concluded that the uncertainty in the parameters and the presence of disturbances have a strong influence on the system. In addition, although the backstepping integral controller is able to reduce the influence of these adverse operating conditions while minimizing the tracking error, the robust PID tuning method uses a simpler model for the system and an algorithm, making the system modelling and controller tuning easier.

The developed platform obtained a satisfactory performance in executing the control systems during the experiments, showing robustness during the executions. In addition, the platform structure can be generalized to any type of car-like four-wheeled electric vehicle, and

the control system can be used to trajectory tracking.

5.1 Future Works

As future work, it would be interesting to study a method to robustify the integral backstepping to some uncertainties. The Backstepping method is based on feedback cancellations and, if we do not cancel some nonlinearities, it may help with the stability of the closed-loop system.

Another extension would be to develop a method to the robust PID tuning without use an iterative algorithm, transforming the BMI problem to an LMI by the use of some assumptions and/or variable changes. Making the method simpler to solve through only one LMI problem.

A study is already being done in relation to the latero-directional dynamics of our robot to provide a two-dimensional trajectory tracking to the system, in uneven terrain conditions. With this, the platform must be improved with new sensors to estimate lateral displacements and the orientation of the robot, as an IMU and a GPS. We may also incorporate a state estimation filter to improve the measurement since encoders often introduce dead-reckoning errors in the navigation.

Thinking about the platform, a method for detecting obstacles, using cameras, lasers and other sensors, would be a future contribution to the project.

As the longitudinal model can be used for platforms with another architecture (differential, for example), experiments in this direction will be considered in the future.

In the future, we intend to start a study related to multi-robot cooperation. Working with multiple of these platforms to perform tasks in formation.

BIBLIOGRAPHY

Alcala, E., Puig, V., Quevedo, J., Escobet, T., and Comasolivas, R. (2018). Autonomous vehicle control using a kinematic lyapunov-based technique with lqr-lmi tuning. *Control Engineering Practice*, 73:1–12. Cited on page 18.

Amer, N. H., Zamzuri, H., Hudha, K., and Kadir, Z. A. (2017). Modelling and control strategies in path tracking control for autonomous ground vehicles: A review of state of the art and challenges. *Journal of Intelligent & Robotic Systems*, 86(2):225–254. Cited 2 times on pages 17 and 20.

Ang, K. H., Chong, G., and Li, Y. (2005). Pid control system analysis, design, and technology. *IEEE transactions on control systems technology*, 13(4):559–576. Cited on page 29.

Attia, R., Orjuela, R., and Basset, M. (2014). Combined longitudinal and lateral control for automated vehicle guidance. *Vehicle System Dynamics*, 52(2):261–279. Cited on page 17.

Bahadorian, M., Savkovic, B., Eaton, R., and Hesketh, T. (2011). Toward a robust model predictive controller applied to mobile vehicle trajectory tracking control. *IFAC Proceedings Volumes*, 44(1):13552–13557. Cited on page 17.

Bennis, N., Duplaix, J., Enéa, G., Haloua, M., and Youlal, H. (2008). Greenhouse climate modelling and robust control. *Computers and Electronics in Agriculture*, 61(2):96 – 107. Cited on page 17.

Boyd, S., El Ghaoui, L., Feron, E., and Balakrishnan, V. (1994). *Linear matrix inequalities in system and control theory*, volume 15. Siam. Cited 3 times on pages 29, 30, and 32.

Cao, Y.-Y., Lam, J., and Sun, Y.-X. (1998). Static output feedback stabilization: an ILMI approach. *Automatica*, 34(12):1641–1645. Cited 5 times on pages 30, 31, 33, 42, and 43.

Cariou, C., Lenain, R., Thuilot, B., and Berducat, M. (2009). Automatic guidance of a four-wheel-steering mobile robot for accurate field operations. *Journal of Field Robotics*, 26(6-7):504–518. Cited on page 18.

Chaibet, A., Nouveliere, L., Mammar, S., and Netto, M. (2005). Backstepping control synthesis for automated low speed vehicle. In *Proc. of the American Control Conf.*, pages 447–452. Cited on page 33.

Chang, X.-H. (2014). *Robust output feedback H-infinity control and filtering for uncertain linear systems*, volume 7. Springer Science & Business. Cited 2 times on pages 31 and 32.

Cheein, F. A. A. and Carelli, R. (2013). Agricultural robotics: Unmanned robotic service units in agricultural tasks. *IEEE Industrial Electronics Magazine*, 7(3):48–58. Cited on page 15.

Chen, C.-T. (1998). *Linear system theory and design*. Oxford University Press, Inc. Cited 4 times on pages 23, 24, 27, and 28.

Costa, F. G., Ueyama, J., Braun, T., Pessin, G., Osório, F. S., and Vargas, P. A. (2012). The use of unmanned aerial vehicles and wireless sensor network in agricultural applications. In *2012 IEEE International Geoscience and Remote Sensing Symposium*, pages 5045–5048. IEEE. Cited on page 14.

Craig, J. J. (2004). *Introduction to Robotics: Mechanic and Control*. Pearson, 3th edition. Cited on page 52.

Dias, J. E. A., Pereira, G. A. S., and Palhares, R. M. (2015). Longitudinal model identification and velocity control of an autonomous car. *IEEE Trans. on Intelligent Transportation Systems*, 16(2):776–786. Cited 2 times on pages 15 and 18.

Dos Santos, F. N., Sobreira, H., Campos, D., Morais, R., Moreira, A. P., and Contente, O. (2016). Towards a reliable robot for steep slope vineyards monitoring. *Journal of Intelligent & Robotic Systems*, 83(3-4):429–444. Cited on page 17.

Du, H., Zhang, N., and Naghdy, F. (2011). Velocity-dependent robust control for improving vehicle lateral dynamics. *Transportation research part C: emerging technologies*, 19(3):454–468. Cited 2 times on pages 17 and 19.

Fang, Z. and Gao, W. (2011). Adaptive integral backstepping control of a micro-quadrotor. In *2011 2nd International Conference on Intelligent Control and Information Processing*, volume 2, pages 910–915. IEEE. Cited on page 20.

Ferreira, E., Miranda, V., Silva Junior, M., Mozelli, L., and Alves Neto, A. (2018). Aplicação de plataforma android no controle de robôs móveis para inspeção de lavouras. *Congresso Brasileiro de Automática - CBA 2018*. Cited 2 times on pages 16 and 21.

Foster, C. A., Strosser, R. P., Peters, J., and Sun, J.-Q. (2005). Automatic velocity control of a self-propelled windrower. *Computers and electronics in agriculture*, 47(1):41–58. Cited on page 18.

Franklin, G. F., Powell, J. D., and Emami-Naeini, A. (2014). *Feedback control of dynamic systems*. Prentice Hall Press. Cited 2 times on pages 27 and 28.

Gat, G., Gan-Mor, S., and Degani, A. (2016). Stable and robust vehicle steering control using an overhead guide in greenhouse tasks. *Computers and Electronics in Agriculture*, 121:234–244. Cited on page 19.

Ge, M., Chiu, M.-S., and Wang, Q.-G. (2002). Robust PID controller design via LMI approach. *Journal of Process Control*, 12(1):3–13. Cited on page 39.

Gray, A., Gao, Y., Hedrick, J. K., and Borrelli, F. (2013). Robust predictive control for semi-autonomous vehicles with an uncertain driver model. In *2013 IEEE Intelligent Vehicles Symposium (IV)*, pages 208–213. IEEE. Cited on page 19.

He, Y. and Wang, Q.-G. (2006). An improved ILMI method for static output feedback control with application to multivariable PID control. *IEEE Trans. on Automatic Control*, 51(10):1678–1683. Cited 5 times on pages 31, 33, 39, 42, and 43.

Herzog, R. and Keller, J. (2011). *Advanced Control: An Overview on Robust Control*. Master of Science in Engineering. Cited on page 26.

Jo, K., Kim, J., Kim, D., Jang, C., and Sunwoo, M. (2014). Development of autonomous car—part i: Distributed system architecture and development process. *IEEE Transactions on Industrial Electronics*, 61(12):7131–7140. Cited on page 15.

Jo, K., Kim, J., Kim, D., Jang, C., and Sunwoo, M. (2015). Development of autonomous car—part ii: A case study on the implementation of an autonomous driving system based on distributed architecture. *IEEE Transactions on Industrial Electronics*, 62(8):5119–5132. Cited on page 17.

Kayacan, E., Ramon, H., and Saeys, W. (2016). Robust trajectory tracking error model-based predictive control for unmanned ground vehicles. *IEEE/ASME Trans. on Mechatronics*, 21(2):806–814. Cited on page 19.

Khalil, H. K. and Grizzle, J. (2002). *Nonlinear systems, vol. 3*. Cited 7 times on pages 23, 24, 33, 34, 35, 45, and 47.

Kong, J., Pfeiffer, M., Schildbach, G., and Borrelli, F. (2015). Kinematic and dynamic vehicle models for autonomous driving control design. In *2015 IEEE Intelligent Vehicles Symposium (IV)*, pages 1094–1099. IEEE. Cited on page 18.

Krstic, M., Kanellakopoulos, I., and Kokotovic, P. V. (1995). *Nonlinear and adaptive control design*. Wiley. Cited 6 times on pages 23, 25, 33, 34, 35, and 47.

Li, J. and Li, Y. (2011). Dynamic analysis and pid control for a quadrotor. In *2011 IEEE International Conference on Mechatronics and Automation*, pages 573–578. IEEE. Cited on page 29.

Löfberg, J. (2004). Yalmip: A toolbox for modeling and optimization in matlab. In *Proceedings of the CACSD Conference*, volume 3. Taipei, Taiwan. Cited on page 30.

Low, C. B. and Wang, D. (2005). Robust path following of car-like wmr in the presence of skidding effects. In *IEEE International Conference on Mechatronics, 2005. ICM'05.*, pages 864–869. IEEE. Cited on page 19.

Mian, A. A., Ahmad, M. I., and Wang, D. (2008). Backstepping based pid control strategy for an underactuated aerial robot. *IFAC Proceedings Volumes*, 41(2):15636–15641. Cited 2 times on pages 45 and 47.

Miranda, V., Alves Neto, A., and Mozelli, L. A. (2018). Estudo sobre estratégias de controle longitudinal para robôs terrestres em terrenos irregulares com inclinação. *Congresso Brasileiro de Automática - CBA 2018*. Cited 2 times on pages 21 and 22.

Mosek, A. (2015). The mosek optimization toolbox for matlab manual. Cited on page 30.

Mozelli, L. A. (2008). Controle fuzzy para sistemas takagi-sugeno: Condições aprimoradas e aplicações. 2008. 87 f. Master's thesis, Dissertação.(Mestrado em Engenharia Elétrica)–Escola de Engenharia .... Cited on page 29.

Mozelli, L. A. and Souza, F. O. (2016). PID design via LMIs: Improved transient response with robustness. In Witrant, E., Fridman, E., Sename, O., and Dugard, L., editors, *Recent results on time-delay systems: analysis and control*, chapter 14, pages 255–274. Springer, 1st edition. Cited on page 29.

Oliveira, A. I., Prado, M. G., and Leite, A. C. (2018). Adaptação de um automodelo para aplicações de robótica móvel na agricultura. *Congresso Brasileiro de Automática - CBA 2018*. Cited on page 18.

Pacejka, H. (2005). *Tire and vehicle dynamics*. Elsevier. Cited on page 37.

Pacejka, H. B. and Bakker, E. (1992). The magic formula tyre model. *Vehicle system dynamics*, 21(S1):1–18. Cited on page 37.

Rajamani, R. (2011). *Vehicle dynamics and control*. Springer Science & Business Media. Cited on page 37.

Rashad, R., Aboudonia, A., and El-Badawy, A. (2015). Backstepping trajectory tracking control of a quadrotor with disturbance rejection. In *2015 XXV International Conference on Information, Communication and Automation Technologies (ICAT)*, pages 1–7. IEEE. Cited 2 times on pages 45 and 47.

Rudol, P. and Doherty, P. (2008). Human body detection and geolocalization for uav search and rescue missions using color and thermal imagery. In *2008 IEEE aerospace conference*, pages 1–8. Ieee. Cited on page 14.

Ruiz-Larrea, A., Roldán, J. J., Garzón, M., del Cerro, J., and Barrientos, A. (2016). A ugv approach to measure the ground properties of greenhouses. In *Robot 2015: Second Iberian Robotics Conf.*, pages 3–13. Springer. Cited on page 17.

Salierno, G. F. and Raffo, G. V. (2017). Whole-body backstepping control with integral action of a quadrotor uav. In *Proceedings of the XIII Brazilian Symposium on Intelligent Automation (SBAI 2017), Porto Alegre, Brazil*, pages 2157–2164. Cited on page 20.

Schmale III, D. G., Dingus, B. R., and Reinholtz, C. (2008). Development and application of an autonomous unmanned aerial vehicle for precise aerobiological sampling above agricultural fields. *Journal of Field Robotics*, 25(3):133–147. Cited on page 14.

Skjetne, R. and Fossen, T. I. (2004). On integral control in backstepping: Analysis of different techniques. In *Proceedings of the 2004 American Control Conference*, volume 2, pages 1899–1904. IEEE. Cited 2 times on pages 45 and 47.

Sturm, J. F. (1999). Using sedumi 1.02, a matlab toolbox for optimization over symmetric cones. *Optimization methods and software*, 11(1-4):625–653. Cited on page 30.

Thanok, S. and Parnichkun, M. (2015). Longitudinal control of an intelligent vehicle using particle swarm optimization based sliding mode control. *Advanced Robotics*, 29(8):525–543. Cited on page 17.

Tomic, T., Schmid, K., Lutz, P., Domel, A., Kassecker, M., Mair, E., Grixa, I. L., Ruess, F., Suppa, M., and Burschka, D. (2012). Toward a fully autonomous uav: Research platform for indoor and outdoor urban search and rescue. *IEEE robotics & automation magazine*, 19(3):46–56. Cited on page 14.

VanAntwerp, J. G. and Braatz, R. D. (2000). A tutorial on linear and bilinear matrix inequalities. *Journal of process control*, 10(4):363–385. Cited on page 31.

Velasquez, A., Higuti, V., Borrero GUerrero, H., Milori, D., Magalhães, D., and Becker, M. (2016). Helvis - a small-scale agricultural mobile robot prototype for precision agriculture. In *Proc. of the 13th Int. Conf. on Precision Agriculture*, pages 1–17, St. Louis, USA. Cited on page 15.

Wit, J., Crane III, C. D., and Armstrong, D. (2004). Autonomous ground vehicle path tracking. *Journal of Robotic Systems*, 21(8):439–449. Cited on page 17.

Wu, X., Jin, P., Zou, T., Qi, Z., Xiao, H., and Lou, P. (2019). Backstepping trajectory tracking based on fuzzy sliding mode control for differential mobile robots. *Journal of Intelligent & Robotic Systems*, pages 1–13. Cited on page 20.

Zhang, F. (2006). *The Schur complement and its applications*, volume 4. Springer Science & Business Media. Cited on page 29.

Zhang, G. and Furusho, J. (2000). Speed control of two-inertia system by pi/pid control. *IEEE Transactions on industrial electronics*, 47(3):603–609. Cited on page 29.

Zhang, H., Shi, Y., and Mehr, A. S. (2012). Robust $\mathscr{H}_\infty$ PID control for multivariable networked control systems with disturbance/noise attenuation. *Int. Journal of Robust and Nonlinear Control*, 22(2):183–204. Cited on page 39.

Zheng, F., Wang, Q.-G., and Lee, T. H. (2002). On the design of multivariable PID controllers via LMI approach. *Automatica*, 38(3):517–526. Cited 3 times on pages 40, 41, and 42.

Zheng, Y., Li, S. E., Wang, J., Cao, D., and Li, K. (2016). Stability and scalability of homogeneous vehicular platoon: Study on the influence of information flow topologies. *IEEE Trans. on Intelligent Transportation Systems*, 17(1):14–26. Cited 2 times on pages 37 and 39.

Zhou, H. and Liu, Z. (2010). Vehicle yaw stability-control system design based on sliding mode and backstepping control approach. *IEEE Transactions on Vehicular Technology*, 59(7):3674–3678. Cited on page 20.

Zhou, K. and Doyle, J. C. (1998). *Essentials of robust control*, volume 104. Prentice hall Upper Saddle River, NJ. Cited 2 times on pages 25 and 30.

Zhou, K., Doyle, J. C., Glover, K., et al. (1996). *Robust and optimal control*, volume 40. Prentice hall New Jersey. Cited 2 times on pages 31 and 32.

Ziegler, J. G. and Nichols, N. B. (1942). Optimum settings for automatic controllers. *trans. ASME*, 64(11). Cited on page 29.